Forschungszentrum Karlsruhe

Technik und Umwelt

Wissenschaftliche Berichte

FZKA 6622

Investigations on the Passive Containment Cooling System of an Advanced Chinese PWR

S. S. Tan*, G. J. Leng*, H. J. Neitzel, H. Schmidt, X. Cheng

Institut für Kern- und Energietechnik
Programm Nukleare Sicherheitsforschung

*Nuclear Power Institute of China, Chengdu

Forschungszentrum Karlsruhe GmbH, Karlsruhe
2001

Impressum der Print-Ausgabe:

Als Manuskript gedruckt

Forschungszentrum Karlsruhe GmbH
Postfach 3640, 76021 Karlsruhe

Mitglied der Hermann von Helmholtz-Gemeinschaft
Deutscher Forschungszentren (HGF)

ISSN 0947-8620

Abstract

Experimental investigations on the thermal-hydraulic performance of the passive containment cooling system (PCCS) of the AC-PWR, which is designed by the Nuclear Power Institute of China (NPIC), are carried out at the PASCO test facility of the Research Center Karlsruhe (FZK). Tests have been performed to study the effect of different baffle types, the wall emissivity, the channel dimension and the water spray on the heat removal. In addition, numerical analysis is performed by the FLUTAN code. Both experimental data and numerical results related to the distribution of the air temperature, the air velocity and the wall temperature are presented and discussed. A satisfying agreement between the numerical results and the experimental data is achieved. It has been found that the effect of the different baffle types and the effect of the channel depth on the total heat removal is negligibly small, whereas a strong effect of the wall emissivity is obtained. The total heat removal is improved significantly by using water spray onto the heated wall surface.

Untersuchungen für ein passives Containment-Kühlsystem eines fortgeschrittenen chinesischen Druckwasserreaktors

Kurzfassung

Am Nuclear Power Institute of China (NPIC) wird ein passives Containment-Kühl-System entworfen, welches auf seine Machbarkeit untersucht werden soll. Dazu wurden am PASCO-Prüfstand des Forschungszentrums Karlsruhe (FZK) experimentelle Untersuchungen zur Wärmeabfuhr von einer beheizten Wand durchgeführt. Der PASCO-Kanal wurde zu diesem Zweck durch Anbringen einer Zwischenwand so abgeändert, dass die Luft durch einen kalten Kanal abwärts strömt, unten umgelenkt wird und durch den beheizten Kanal nach oben strömt. Ziel der experimentellen Untersuchungen war es, die Einflüsse unterschiedlicher Zwischenwand-Typen, der thermischen Emissionskoeffizienten der Wände, der Kanal-Tiefe sowie eines Wasser-Sprüh-Systems auf die Wärmeabfuhr zu studieren. Mit dem FLUTAN-Rechenprogramm wurden numerische Analysen durchgeführt. Experimentelle und numerische Ergebnisse bezüglich der Verteilung von Temperatur und Geschwindigkeit der Luft im Kanal werden dargestellt. Es konnte eine genügend gute Übereinstimmung zwischen Rechnung und Experiment erreicht werden. Es ergab sich, dass unterschiedliche Zwischenwand-Typen nahezu keine Auswirkung auf die gesamte Wärmeabfuhr an die Luft haben. Der Einfluss der Kanal-Tiefe ist ebenfalls gering, während sich die Emissionskoeffizienten der Wände stark auswirken. Schließlich ist die Verwendung eines Wasser-Sprüh-Systems für die Wärmeabfuhr von der beheizten Wand außerordentlich wirksam.

Contents

1 Introduction

In order to meet the increasing demand of power supply, different kinds of advanced water cooled reactors have been proposed where the concept of passive safety has been widely used [1]. The use of passive safety features will simplify the system and increase the reliability of the performance of essential safety functions. In this way it will improve the public acceptance of nuclear energy. Relating to the passive containment cooling system, a lot of experimental and analytical studies have been carried out, especially in USA and in Europe, e.g. PASCO program at the Forschungszentrum Karlsruhe (FZK), Germany [2-5]. Based on the test results, some computer codes have been developed.

Since the middle 1980s, Nuclear Power Institute of China (NPIC) started the design of the new generation water-cooled reactors: Advanced Chinese Pressurized Water Reactor (AC-PWR) which applies passive safety systems in order to increase the safety of plants and reduce the construction cost [6, 7]. The passive safety systems include passive emergency core cooling system (PECCS) [8], passive residual heat removal system (PRHRS) and passive containment cooling system (PCCS) [9], only rely on natural force, gravity, condensation and evaporation. In comparison with the conventional reactor, the AC-PWR has some new features:

- Lower capital cost and shorter construction time;
- Simpler and easier to operate;
- Higher availability and longer operating life;
- Reduction of the possibility of core meltdown;
- Minimum effect on the environment;
- Module design.

The passive containment cooling system is one of the important parts of the passive safety system in the AC-PWR, as shown in figure 1.1. It consists of an inner steel shell of about 38 m diameter and 40 mm wall thickness and an outer reinforced concrete shell of about 40m diameter and 2 m wall thickness. There is an annulus gap between the two shells, the gap is divided by an air-guiding plate (i.e. baffle). There are 15 air inlet holes around the top of the concrete wall. The air outlet (chimney) is located at the center of the top of the concrete wall. A water storage tank is located around the chimney and provides water spray to the steel shell. The water quantity is enough to cool the steel shell for 3 days. The decay heat in a core meltdown accident is removed by evaporation/condensation and natural air convection coupled with thermal radiation to the ambient atmosphere in a passive way. The steam

temperature and pressure in the containment will be limited below the design value. In this way the consequences of a severe core meltdown accident will be restricted to inside the containment. There will not be any noticeable release of radioactivity impairing the public.

Up to now there is still a big deficiency in reliable knowledge of the thermal-hydraulic performance of such a passive heat removal system. Further experimental and theoretical studies are needed to provide necessary data for designing the passive cooling system and for validating computer codes.

The present study is a joint project of FZK and NPIC [10]. Thermal-hydraulic tests of the passive containment cooling system are performed at the PASCO test facility which is available at FZK. At the same time, numerical analysis is carried out by using the FLUTAN code developed at FZK.

The goal of this project is to study the effect of baffle (air-guiding plate) on the heat removal in the containment air channel, and to study the effect of water film flow on the decay heat removal.

The PASCO experiments will improve the understanding of heat and mass transfer phenomena involved in the passive containment cooling system of the AC-PWR. The experimental data can be used to verify the models in computer codes such as FLUTAN and PCCSAC developed at NPIC.

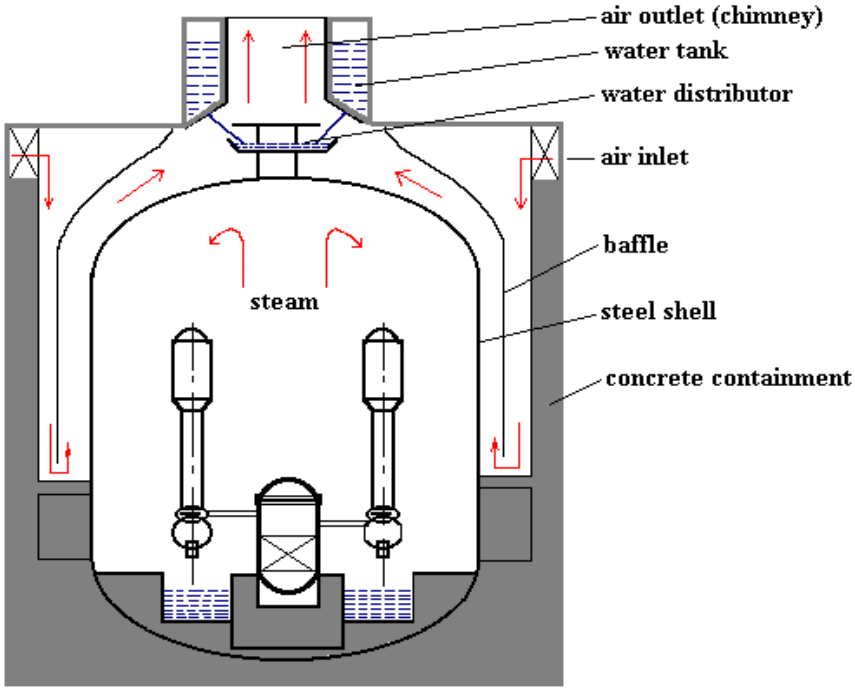

Figure 1.1: Passive containment in AC-PWR

2 Experimental program

2.1 Test facility

The PASCO test facility, shown in figure 2.1, was built at FZK to study the thermal-hydraulic phenomena in the passive containment cooling system of the composite containment [3]. The test section consists of a vertical rectangular channel of which one wall is electrically heated. All the walls are thermally insulated from the ambient surroundings. The width of the channel is 0.5 m, and the maximum channel depth is 1.0 m. The height of the test facility is about 9 m, the maximum heated height is 8 m consisting of four individually heated plates. The heated wall consists of a steel plate with a thickness of 40 mm, an insulating layer with a thickness of 157 mm and an outer aluminium plate with a thickness of about 1 mm, nine heated rods are embedded in each steel plate. The heated wall is positioned by fixing the heated plates to the peripheric structure. The thermal conductivity of

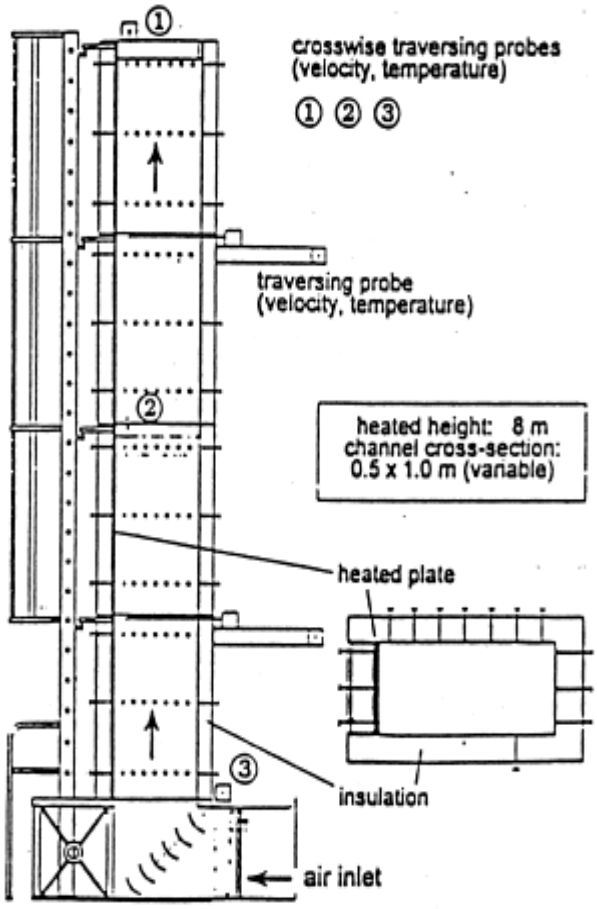

Figure 2.1: PASCO test facility

the insulating material is about 0.01 W/m K. The unheated wall consists of an inner steel plate, an insulating layer and an outer aluminium plate. The thickness of the steel plate and of the aluminium plate is 1 mm. The thickness of the insulating layer is 157 mm. The channel depth, the heated height, the wall emissivity and the temperature of the heated wall can be varied.

Because of the configuration difference between passive containment cooling system of the composite containment, shown in figure 2.2, and that of the AC-PWR, modification of the PASCO test facility was necessary. In the composite containment, the annulus of approx. 80cm radial gap width is bridged by longitudinal support ribs fixed in the concrete shell, the cooling air enters the annulus from the lower part and flows upward in the individual chimneys formed by the support ribs in the annular gap. In AC-PWR, an air baffle is installed between the two shells of the containment to enable the air flowing into the cooling channel from the upper part. A water tank is placed above the steel shell of the containment to form the cooling water film on the steel shell. Therefore, the following modifications were taken for the present study, shown in figure 2.3:

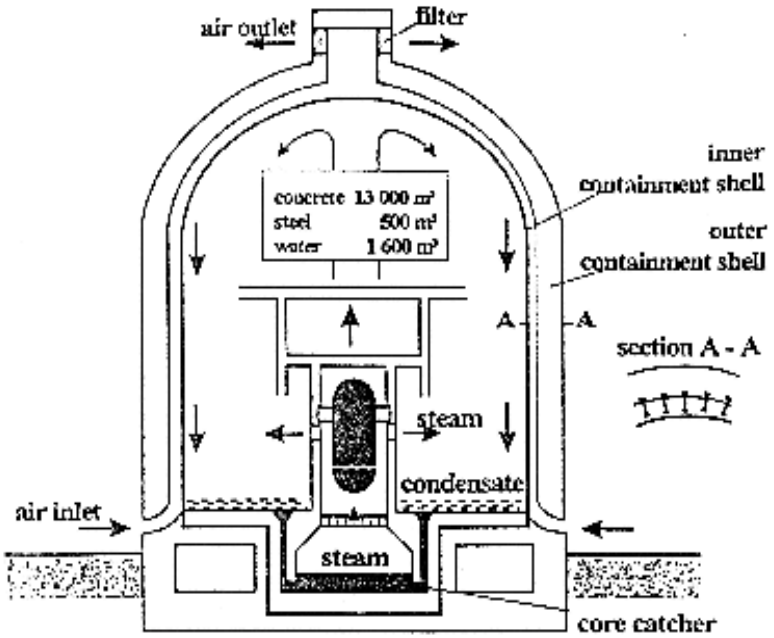

Figure 2.2: Composite containment in Germany

a. <u>Installation of the baffle</u>

A thermally conducting or insulating baffle is added in the channel to change the location of the air inlet. The whole channel of the test facility is divided into two channels by the baffle,

i.e. a cold channel and a hot channel. The thermally conducting baffle consists of a steel plate with a thickness of 3 mm. The thermally insulating baffle consists of two steel plates and an insulating layer between the steel plates. The thickness of the steel plate is 1 mm, and the thickness of the insulating layer is 78 mm. The height of the baffle is 6.0 m consisting of three individual parts. The width of the baffle is 0.5 m. In order to study the effect of the channel dimension, the channel depth between the baffle and the heated wall can be changed by moving the baffle.

b. <u>Inlet cross section</u>

The Inlet of cooling air is located at the top of the containment in an AC-PWR. The original air inlet of the PASCO test facility was closed by a steel plate.

To prevent mixing of the air flowing in and out, the inlet and outlet cross section are located at different elevations. The inlet cross section locates at Z=6m, whereas the outlet cross section is at Z=8m.

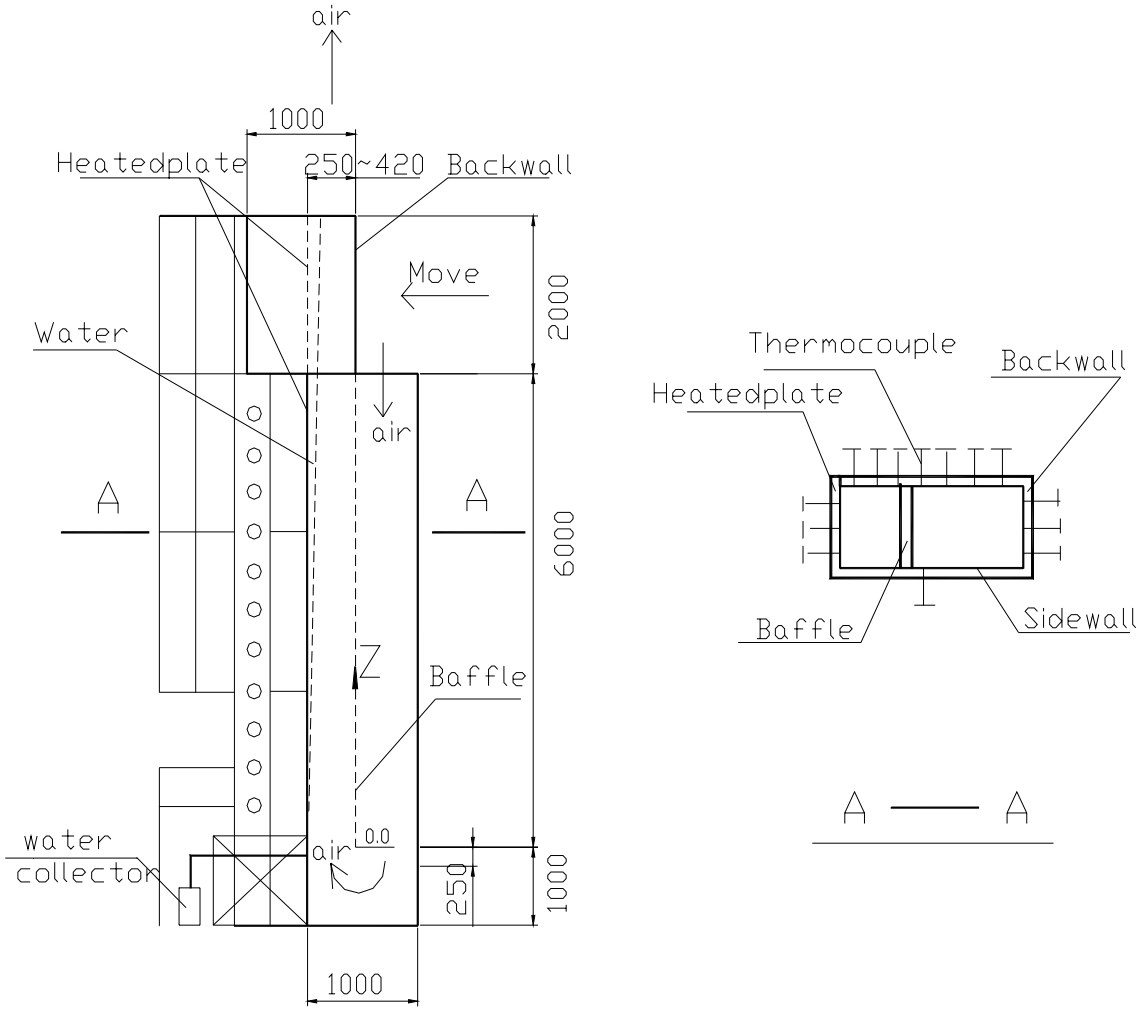

Figure 2.3: Modified PASCO test facility

c. Minimization of radiation of the side wall

In AC-PWR, radiative heat transfer takes place between the steel shell, the baffle and the concrete shell, no side walls are present. Therefore, the radiative effect of the side wall should be minimized in the PASCO experiment. For this reason, the wall emissivity of the side wall is as small as possible. In the present study the wall emissivity of the side walls is 0.4.

d. Water collector for the tests under wet conditions

For heat transfer tests under wet conditions, a water collector is installed at the bottom of the heated wall to collect the discharged water.

Figure 2.4 shows the photograph of the modified PASCO test facility.

Figure 2.4: Photograph of the modified PASCO test facility

2.2 Measurement instrumentation

The test facility is equipped with approx. 170 thermocouples to measure the distribution of the wall temperatures. The air temperature and the air velocity are measured by traversing probes installed at different elevations. Thermocouples installed on the baffle surface measure the temperature distribution on the baffle. The vaporization quantity of the water film can be obtained from the water flow rate at the inlet minus the discharged water flow rate. The main test parameters measured are summarized as below:

a. Wall temperatures

Temperatures of the heated wall, the side wall, the back wall and the baffle are measured in 36, 76, 36, 15 measuring points, respectively. All the wall temperatures are measured by thermocouples with a measurement accuracy of $\pm 0.75\ ^{0}C$.

b. Air temperature in the channel

The air temperature distribution in the channel is measured by traversing thermocouples installed at four different elevations, i.e. the inlet (Z=6 m), the mid-plane of the cold channel (Z=2 m), the mid-plane of the hot channel (Z=4 m), the outlet (Z=8 m). The measurement accuracy is $\pm 0.75\ ^{0}C$.

c. Air velocity in the channel

The air velocity distribution in the channel is measured by traversing Prandtl-tubes installed at three different elevations, i.e. the mid-plane of the cold channel (Z=2 m), the mid-plane of the hot channel (Z=4 m), the outlet (Z=8 m). The measurement accuracy is ± 2.0 %.

d. Heat power

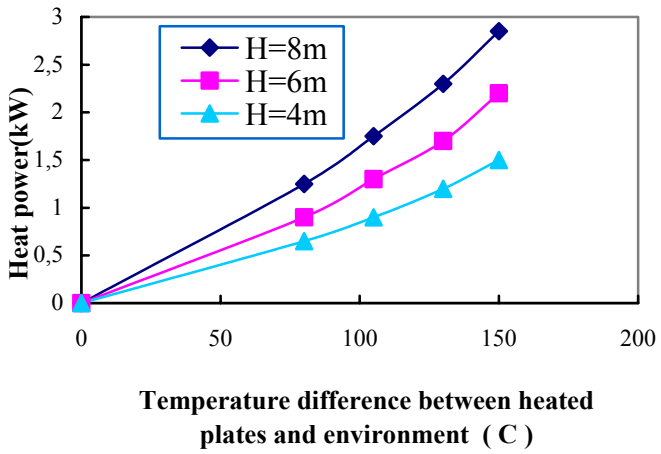

Figure 2.5: Heat loss calibration results (H-Heated height)

To calculate the heat power of the heated wall, the electric current and the voltage of each heated plate are recorded. The measurement accuracy of the heat power is ±1.0 %. The heat transferred to the air flow can be calculated from the total heat power minus the heat loss which is shown in figure 2.5.

e. Evaporation rate of water

The water flow rate at the inlet and the discharged flow rate are measured. The difference between these two values is considered as the amount of vaporized water.

f. Other parameters

The pressure and temperature at the inlet is measured by pressure gauge and thermocouple respectively. The humidity of air at the inlet is measured by a hygrometer.

The measured test parameters are summarized in table 2.1. Z stands for the axial elevation, indicated in figure 3.1 and figure 3.2.

Table 2.1: Measured parameters

Wall temperature (^{0}C) (Number)	$T_{Heated\ wall}$ (36)	$T_{Side\ wall}$ (76)	$T_{Back\ wall}$ (36)	T_{Baffle} (15)
Air temperature distribution(^{0}C)	$T_{Cold\ air(Inlet)}$ (Z=6 m)	$T_{Cold\ air}$ (Z=2 m)	$T_{Hot\ air}$ (Z=4 m)	$T_{Hot\ air(Outlet)}$ (Z=8 m)
Air velocity distribution(m/s)	$V_{Cold\ air}$ (Z=2 m)	$V_{Hot\ air}$ (Z=4 m)	$V_{Hot\ air(Outlet)}$ (Z=8 m)	
Electric current, Voltage (A), (V)	The electric currents and voltages of all heating elements			
Water flow rate (l/min)	Q_{Inlet}	$Q_{Discharged}$		
Inlet parameters	Temperature T_0(^{0}C)	Pressure P_0(Pa)	Humidity Φ_0(%)	

2.3 Test parameters

The tests consist of three parts, i.e. dry tests with a thermally conducting baffle, dry tests with a thermally insulating baffle, and wet tests.

a. Heat transfer tests under dry conditions

The effect of the heated wall temperature, of the channel dimension and of the wall emissivity on the heat transfer is studied. The main test parameters are summarized in table 2.2.

Table 2.2: Matrix of the dry tests

Parameter / Type	Heated wall emissivity	Side wall (Back wall) emissivity	Baffle emissivity	Hot channel dimension (mm)	Heated height (m)	Heated wall temperature (°C)
Dry tests with a conducting baffle	0.9	0.4(0.9)	0.9	330×500	6.0	50, 100, 120,150
					8.0	
Dry tests with an insulating baffle	0.9	0.4(0.9)	0.9	250×500	8.0	50, 100, 120,150
				330×500	6.0	
					8.0	
				420×500	8.0	
	0.4	0.4(0.9)	0.9	250×500	8.0	
				330×500	8.0	
				420×500	8.0	
	0.4	0.4(0.9)	0.4	330×500	8.0	

b. <u>Heat transfer tests under wet conditions</u>

For the heat transfer tests under wet conditions, some modifications were undertaken, i.e. installation of the water collector, coating of Carbo zinc® on the heated wall and on the baffle to improve the distribution of the water film. The main test parameters are summarized in table 2.3.

Table 2.3: Matrix of the wet tests

Parameter / Type	Heated wall emissivity	Side wall (Back wall) emissivity	Baffle emissivity	Hot channel dimension (mm)	Water flow rate (l/min)	Heat power ($kW/m^{2)}$
Wet tests with an insulating baffle	0.85	0.4(0.9)	0.85	420×500 H=8m	0.5~2	2, 3.5, 5

c. <u>Water film observation</u>

The baffle, the back wall and the side walls of the modified PASCO test facility are removed under the condition of no heat power supplied. The distribution of the water film on the heated wall is observed by camera or video camera when the inlet water flow rate changes from 0.5 to 2 l/min.

3 Experimental results

3.1 Distribution of air temperature and air velocity

The cold channel and the hot channel geometry considered are rectangular, vertical channels, as indicated in figure 3.1 and figure 3.2.

Figure 3.3 and figure 3.4 show the profiles of the air temperature and of the air velocity measured at the outlet cross section for the following test conditions: heated height 8.0 m, the hot channel depth 330 mm, the emissivity of the heated wall and of the baffle 0.9, the emissivity of the side wall and of the back wall 0.4, the heated wall temperature 150 ^{0}C and the inlet air temperature 20 ^{0}C. The test was carried out with a thermally insulating baffle. In the region near the heated wall (X=0.33 m), the air temperature and the air velocity reach their maximum values. They decrease rapidly by increasing the distance from the heated wall. Due to thermal radiation between the heated wall and other walls, the air temperature and the air velocity increase again by approaching to the side wall and the baffle. The minimum values of the air temperature and of the air velocity appear in the central region of the cross-section.

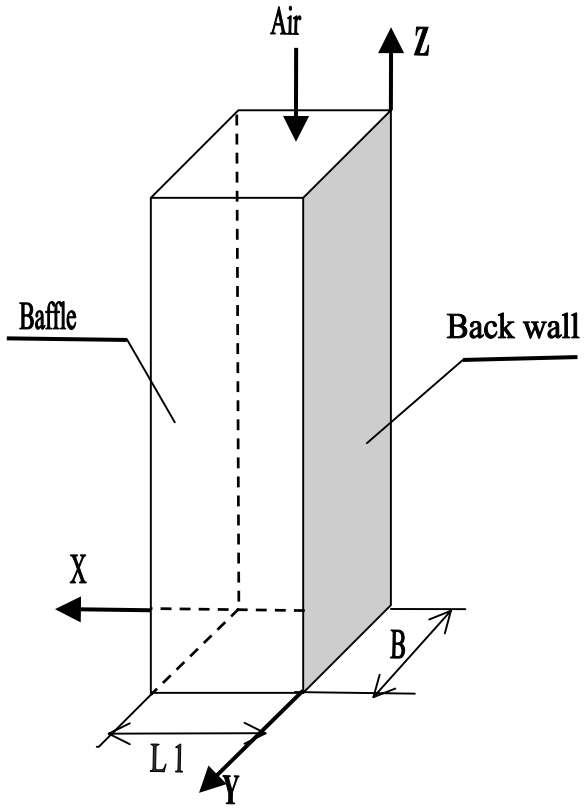

Figure 3.1 : Cold channel

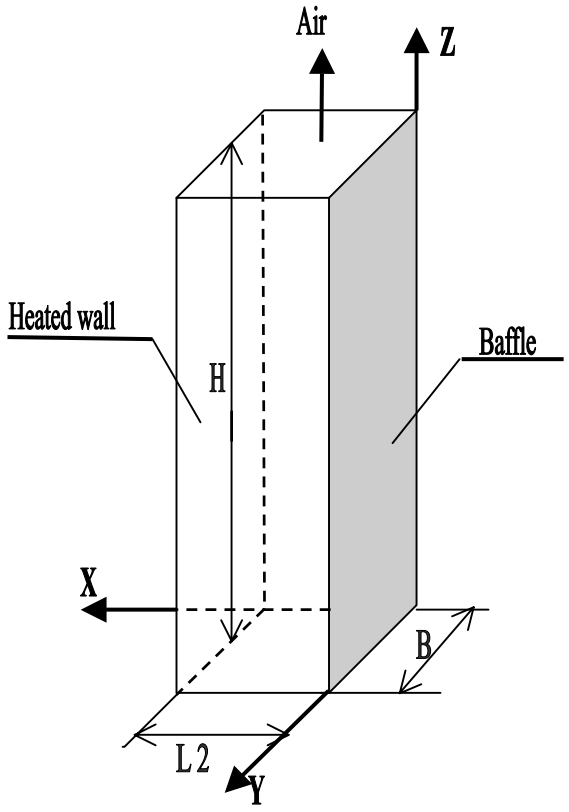

Figure 3.2 : Hot channel

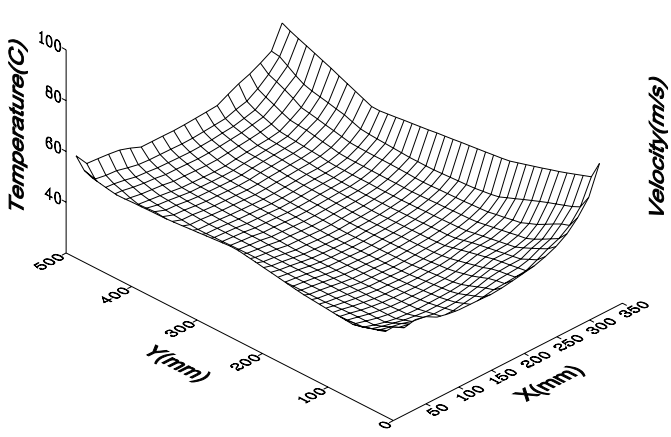

Figure 3.3 : Air temperature profile at the outlet cross-section

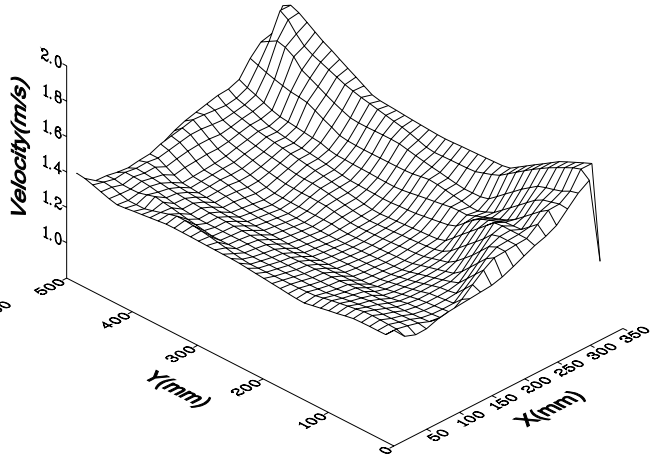

Figure 3.4 : Air velocity profile at the outlet cross-section

Figure 3.5 and figure 3.6 illustrate the air temperature and the air velocity along the mid-line (Y=0.25 m) versus the value of X at different axial levels. The test conditions are the same as above. Due to the existence of the insulating layer in the baffle, the heat conduction through the baffle is negligible small. Therefore, the temperature along the mid-line in the cold channel (at Z=1.8 m) remains nearly unchanged. It is slightly higher than that at the inlet cross section. The maximum velocity appears in the central region, whereas it decreases towards the walls. In the hot channel (Z=3.8 m and Z=7.8 m), the minimum air temperature and air velocity appear in the central region. They increase by approaching to the walls.

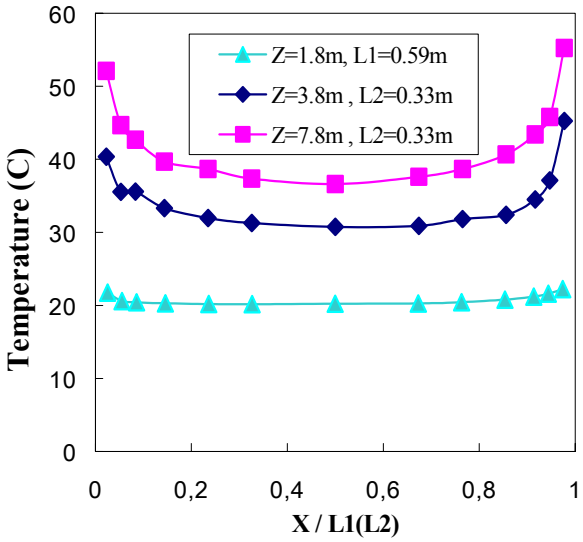

Figure 3.5 : Air temperature distribution (Y=250 mm)

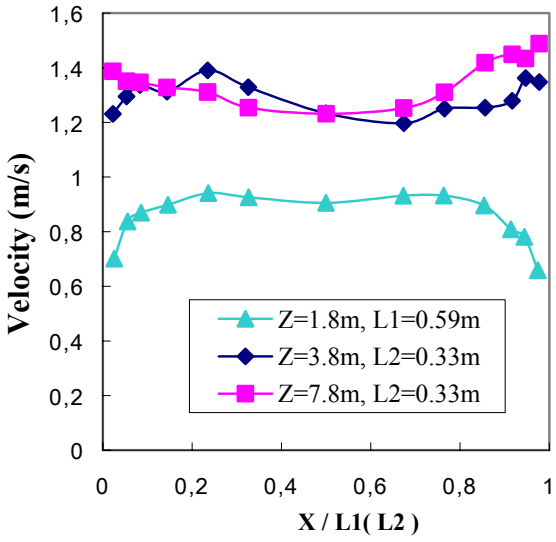

Figure 3.6: Air velocity distribution (Y=250 mm)

Figure 3.7 shows the temperature distribution on the side wall of the cold and of the hot channel at three elevations (Z=1 m, 3 m, 5 m) under the same test conditions as in figure 3.5. Figure 3.8 presents the temperature distribution on the baffle and on the back wall. In the hot channel, due to thermal radiation, the temperature on all walls is much higher than the average air temperature at the same elevation. It is seen that the side wall temperature increases by approaching to the heated wall or by increasing the elevation. The maximum baffle temperature locates at the mid-line of the baffle (Y=0.25 m), and it increases by increasing axial elevation. In the cold channel, the back wall temperature has a uniform distribution and the value is almost the same as the ambient air temperature. The side wall temperature of the cold channel changes slightly and shows only a slight increase in the region near the baffle. Similar results are obtained for other test conditions with a thermally insulating baffle.

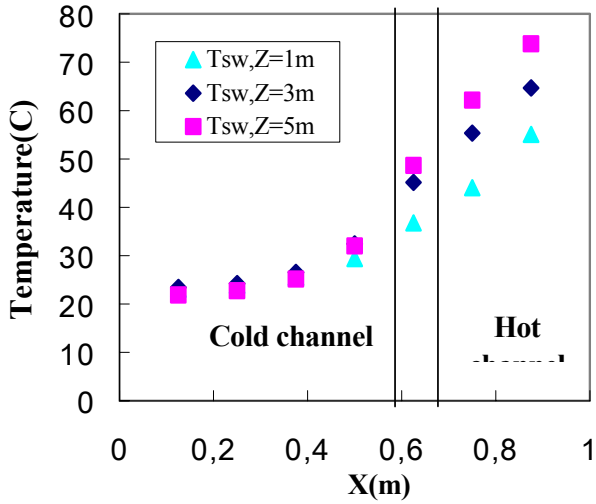

Figure 3.7 : Side wall temperature

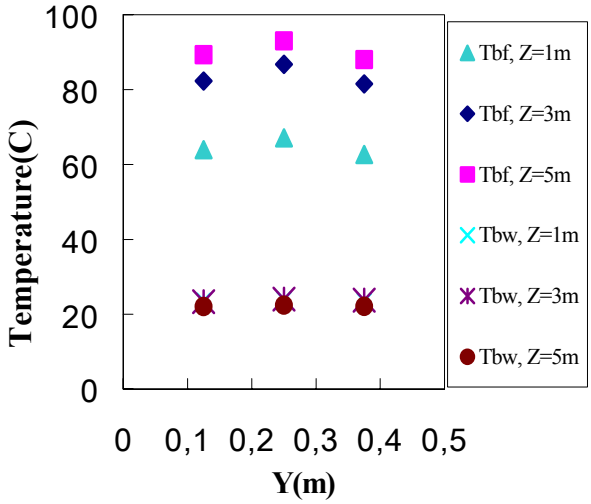

Figure 3.8 : Baffle and back wall temperature

The distribution of the air temperature and of the air velocity at the outlet cross section for a test with a thermally conducting baffle are shown in figure 3.9 and figure 3.10. The test parameters are: heated height 8.0 m, heated wall temperature 150 ^{0}C, heated wall emissivity 0.9, baffle emissivity 0.9, back wall emissivity 0.9, side wall emissivity 0.4, hot channel depth 330mm and inlet air temperature 20 ^{0}C. It can be seen that the maximum values of the air temperature and of the air velocity appear in the region near the heated wall (i.e. X=0.33 m). Both the air temperature and the air velocity decrease by increasing the distance from the heated wall. Due to thermal radiation, the air temperature and the air velocity increase again by approaching to the side wall and the baffle. The minimum values of the air temperature and of the air velocity appear in the central region of the cross-section. In case with a

thermally conducting baffle, some heat is transferred from the hot channel to the cold channel, thus the baffle temperature is lower than that in case with a thermally insulating baffle. For this reason, the air temperature and the air velocity near the baffle change only slightly, especially for the air velocity which remains almost constant.

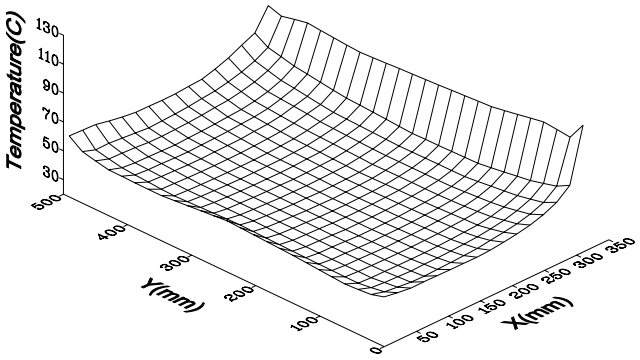

Figure 3.9 : Air temperature profile at the outlet cross-section

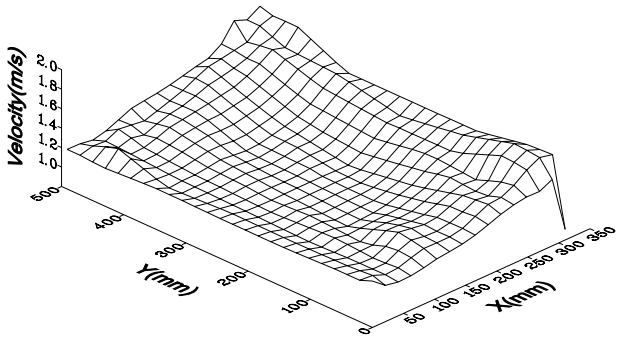

Figure 3.10 : Air velocity profile at the outlet cross-section

Figure 3.11 and figure 3.12 show the air temperature distribution and the air velocity distribution along the mid-line (Y=0.25 m) versus the value of X at different axial elevations under the same test conditions as in figure 3.9. For a thermally conducting baffle, heat transfer

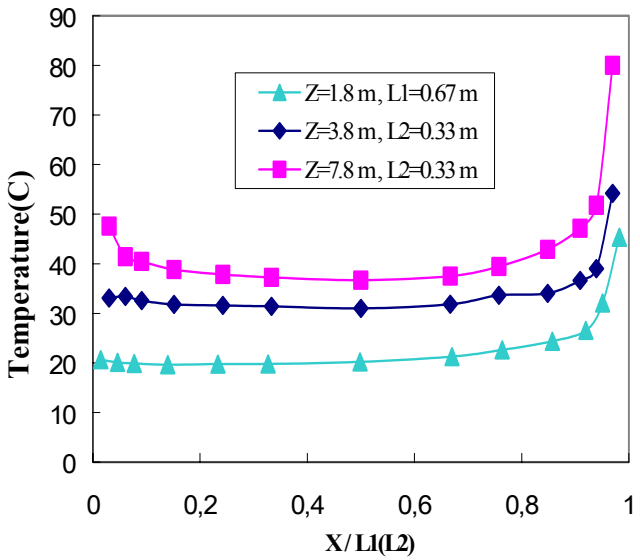

Figure 3.11 : Air temperature distribution (Y=250 mm)

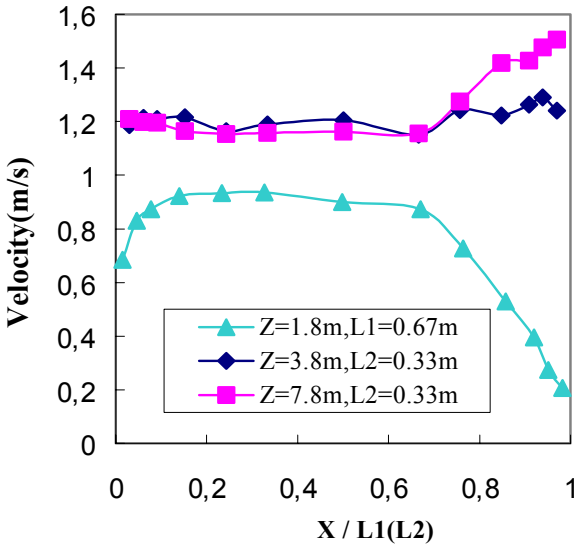

Figure 3.12 : Air velocity distribution (Y=250 mm)

takes place from the hot channel through the baffle to the cold channel. Therefore, it can be seen that the air temperature along the mid-line in the cold channel (at Z=1.8 m) increases by approaching to the baffle (X/L1=1). The maximum value appears in the region near the baffle. The maximum velocity appears in the central region, whereas it decreases in the region near the walls. Because of the buoyancy effect which reduces the downward air flow, a larger decrease in the velocity occurs in the region near the baffle. The minimum velocity is about 0.2 m/s. In the hot channel (Z=3.8 m and Z=7.8 m), the minimum air temperature and the minimum air velocity appear in the central region. Both velocity and temperature increase significantly by approaching to the heated wall (X/L2=1), whereas only a slight increase in velocity and temperature was obtained by approaching to the baffle (X/L2=0).

Figure 3.13 and figure 3.14 illustrate the temperature distribution on the side wall, on the baffle and on the back wall at three elevations (Z=1m, 3m, 5m). In the hot channel, all the unheated wall temperatures are much higher than the average air temperature at the same elevation. The side wall temperature increases by approaching to the heated wall or by increasing the elevation. The maximum baffle temperature locates at the mid-line of the baffle (Y=0.25 m) and increases with the axial elevation. In the cold channel, the back wall temperature has a uniform distribution and the value increases slightly compared to the ambient air temperature. The maximum back wall temperature locates at the mid-line (Y=0.25m). The side wall temperature of the cold channel changes only slightly and increases in the region near the baffle (X=0.67m).

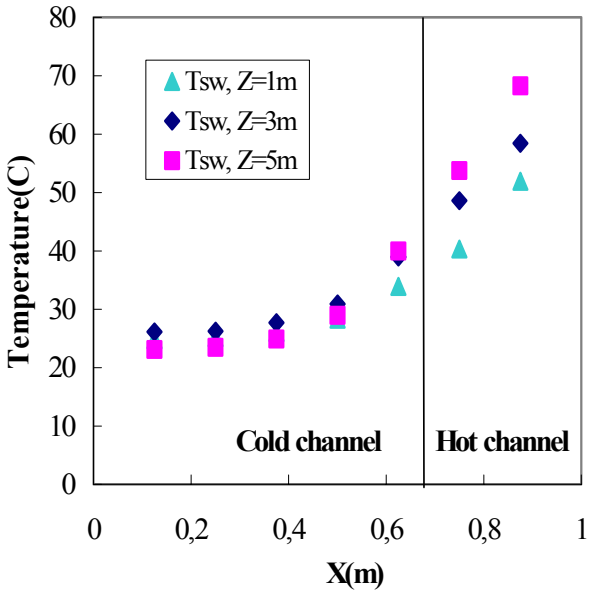

Figure 3.13 : Side wall temperature

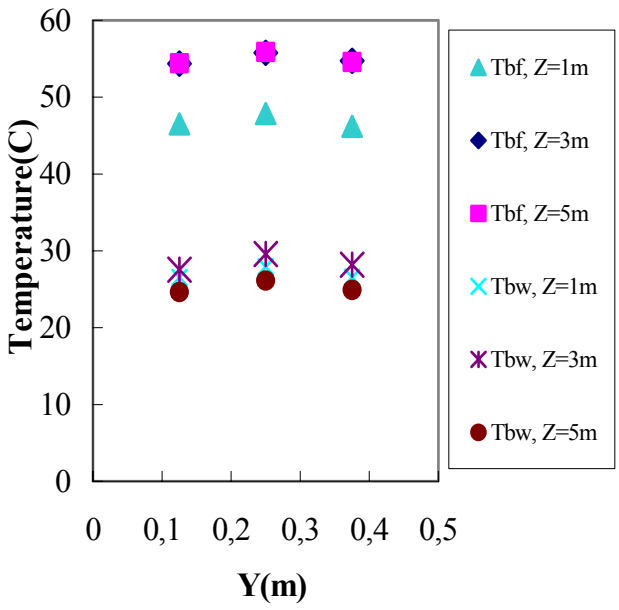

Figure 3.14: Baffle and back wall temperature

3.2 Effect of the channel dimension

To study the influence of the channel dimension, tests were carried out with a thermally insulating baffle and with different channel dimensions. Figure 3.15 and figure 3.16 compare the air temperature distribution and the air velocity distribution along the mid-line (Y=0.25m) of the hot channel outlet. The test parameters are: heated height 8.0 m, heated wall temperature 150^0C, side wall emissivity 0.4, emissivity of other walls 0.9, inlet air temperature 20^0C. Three different dimensions of the hot channel 250×500 (mm), 330×500 (mm) and 420×500 (mm). It is seen that the outlet air temperature changes slightly by changing the hot channel dimension. By reducing the channel dimension, the effect of thermal radiation increases and the radiative heat exchange is enhanced between the heated wall and the back wall. This leads to an increase in the outlet air velocity. In a narrow hot channel, the air velocity has a more uniform distribution along the X-axis.

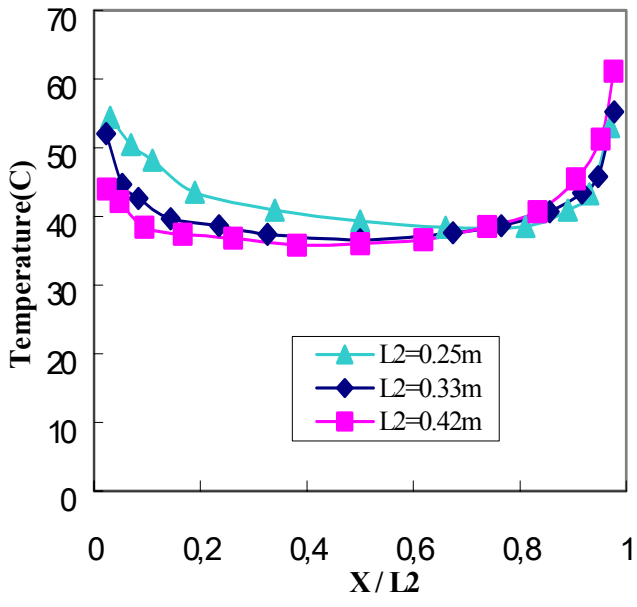

Figure 3.15 : Air temperature distribution (Y=250 mm)

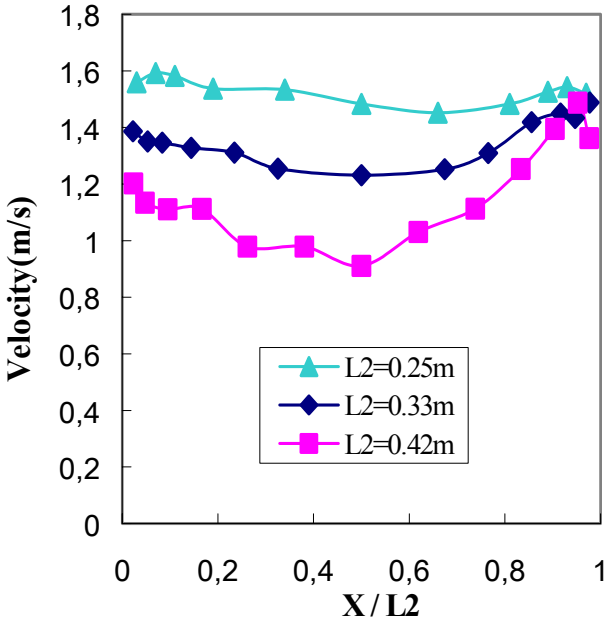

Figure 3.16 : Air velocity distribution (Y=250 mm)

Figure 3.17 and figure 3.18 compare the temperature distribution on the side wall, on the baffle and on the back wall at Z=3m for the three different channel dimensions. It is found that the effect of the channel dimension on the wall temperature is negligibly small. However, this conclusion is only valid for the parameter range considered. A more significant effect of the channel dimension has been found in [3].

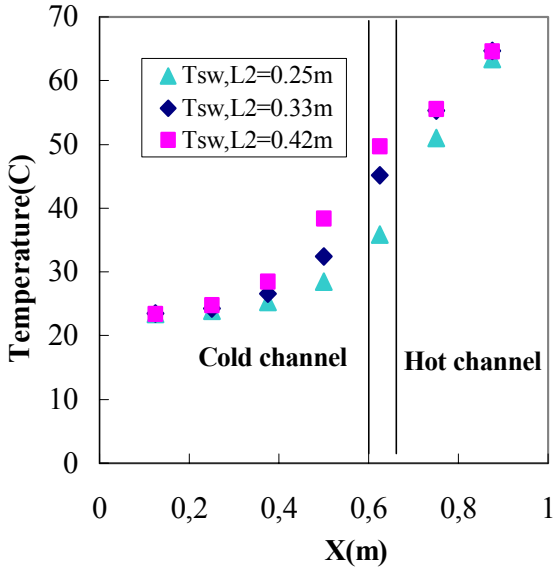

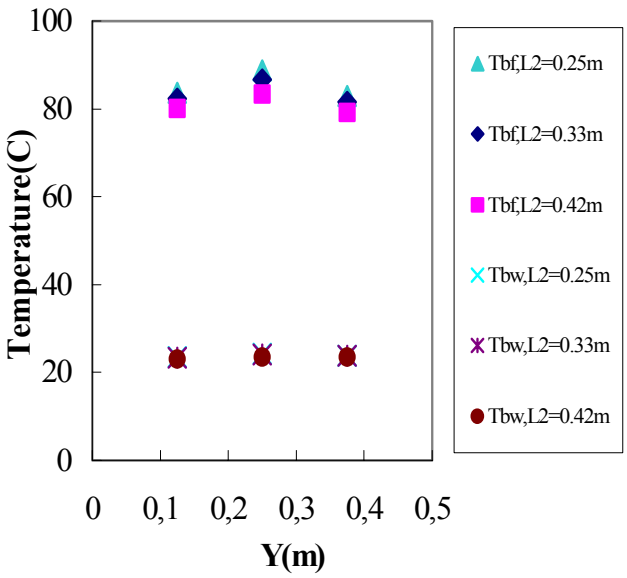

Figure 3.17 : Side wall temperature **Figure 3.18 : Baffle and back wall temperature**

Figure 3.19 shows the air flow rate for three different channel dimensions versus the heated wall temperatures. The other test conditions are the same as indicated in figure 3.15. It is seen that the outlet air mass flow rate increases by increasing the hot channel dimension (from L2=0.25m to L2=0.42m). Figure 3.20 compares the total removed heat for three different channel dimensions under the same test conditions as indicated in figure 3.19. It's found that the influence of the channel dimension on the removed heat power is small. The heat quantity increases only slightly by increasing the hot channel dimension.

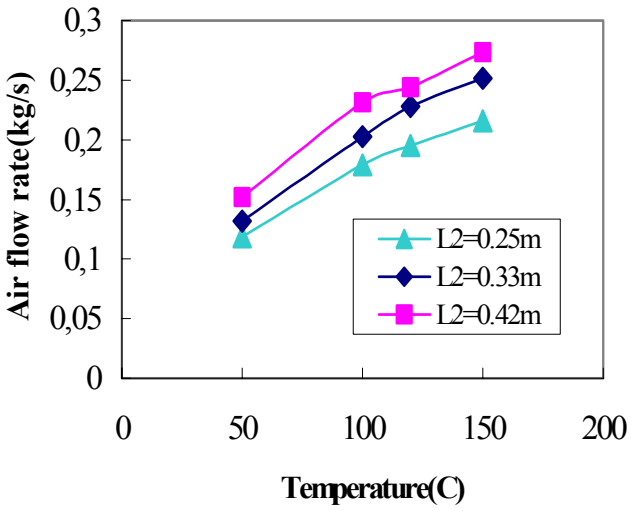

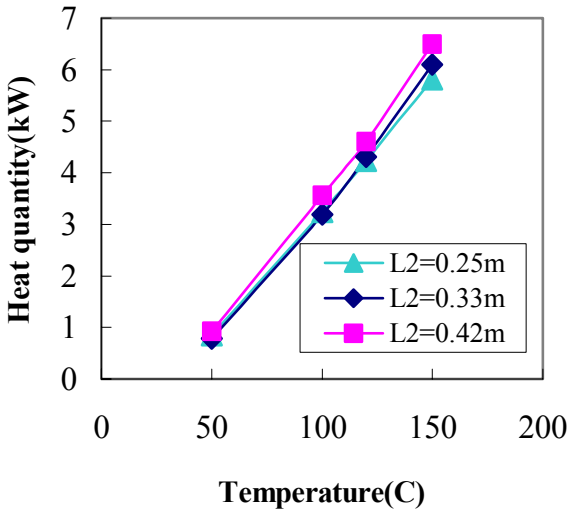

Figure 3.19 : Air mass flow rate for different dimension

Figure 3.20 : Removed heat for different dimension

Figure 3.21 and figure 3.22 compare the outlet mass flow rate and the total removed heat for different channel dimensions (L2=0.25m, 0.33m and 0.42m) at a lower emissivity of the heated wall. The test conditions are: heated height 8.0m, emissivity of the side wall and of the heated wall 0.4, emissivity of other walls 0.9, inlet air temperature 20 ^{0}C. A thermally insulating baffle is used. Similar results as indicated in figure 3.19 and figure 3.20 are obtained.

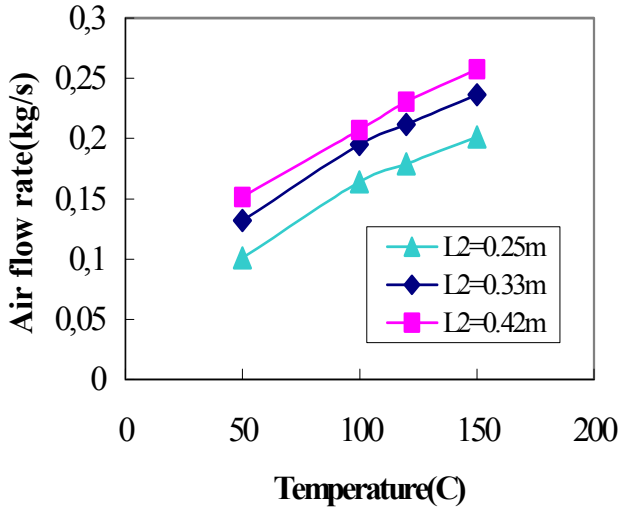

Figure 3.21 : Air mass flow rate for different dimension

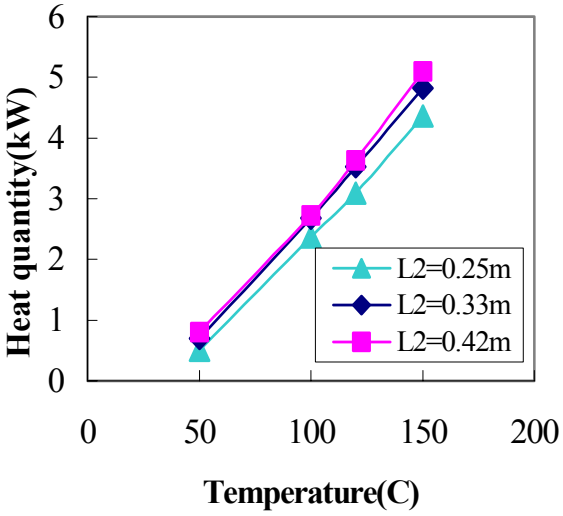

Figure 3.22 : Removed heat for different dimension

3.3 Effect of the wall emissivity

To obtain the effect of the wall emissivity, tests were performed with two different heated wall emissivities (i.e. e1=0.9, 0.4) and with a thermally insulating baffle. Figure 3.23 and figure 3.24 illustrate the air temperature and the air velocity profiles at the outlet cross-section along the mid-line (Y=0.25 m) for the following test conditions: heated height 8.0 m, hot channel dimension 330×500 (mm), heated wall temperature 150 ^{0}C, side wall emissivity 0.4, emissivity of the baffle and of the back wall 0.9, inlet air temperature 20 ^{0}C. It is found that the effect of the thermal radiation increases by increasing the heated wall emissivity. This leads to an increase in the outlet air temperature. For the same reason, the outlet air velocity increases by increasing the heated wall emissivity.

Figure 3.25 shows the temperature on the side wall at Z=3m for the two different heated wall emissivities under the same test conditions as in figure 3.23. It is seen that the temperature on the side wall increases by increasing the heated wall emissivity. In figure 3.26,

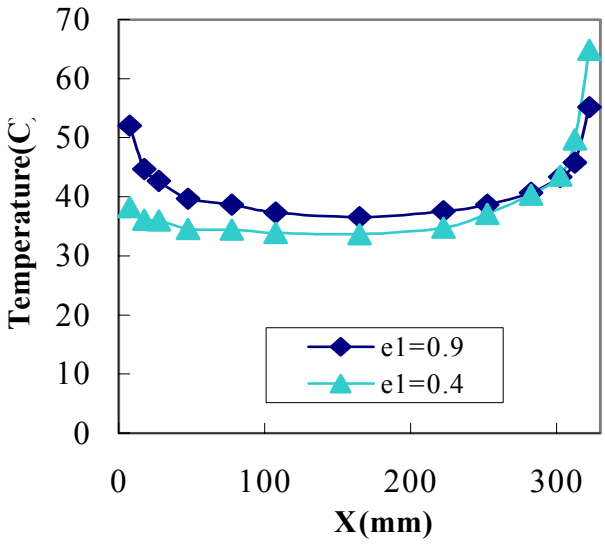

Figure 3.23 : Air temperature distribution (Y=250 mm)

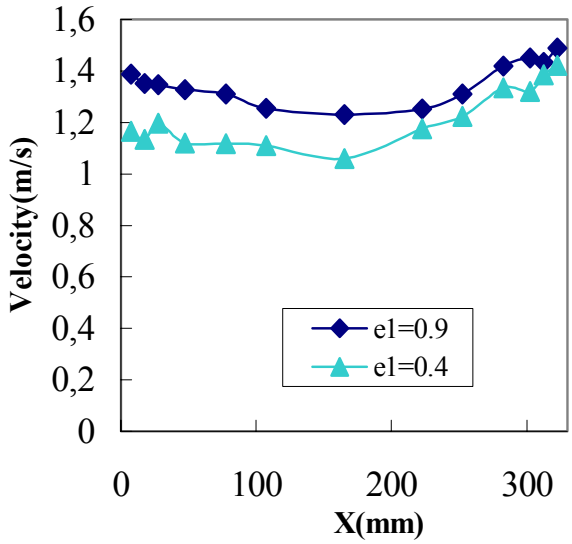

Figure 3.24 : Air velocity distribution (Y=250 mm)

the temperature on the baffle increases significantly by increasing the heated wall emissivity, whereas the temperature on the back wall remains nearly unchanged at Z=3m.

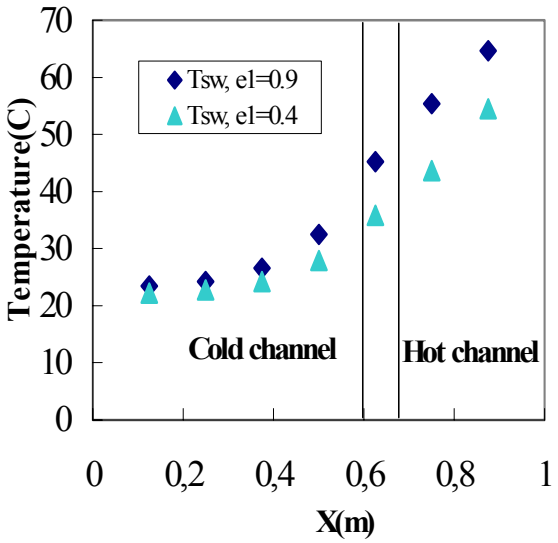

Figure 3.25 : Side wall temperature

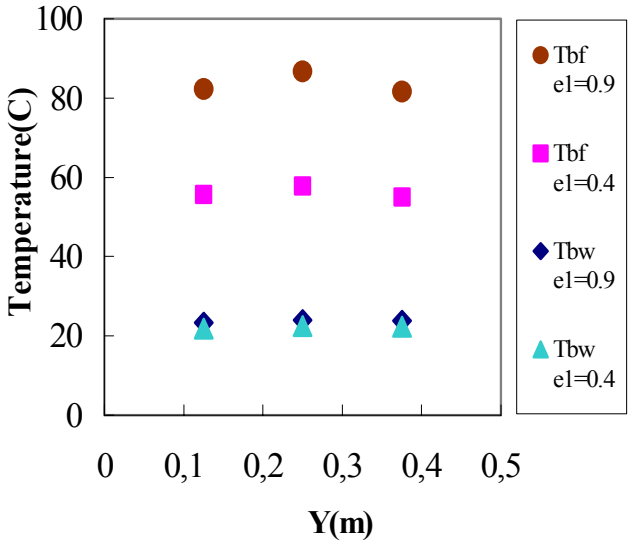

Figure 3.26 : Baffle and back wall temperature

Figure 3.27 and figure 3.28 compare the outlet air flow rate and the removed heat for the two different heated wall emissivities (e1=0.9, 0.4), the test conditions are the same as in figure 3.23. It is found that both the mass flow rate and the removed heat increase by

increasing the heated wall emissivity.

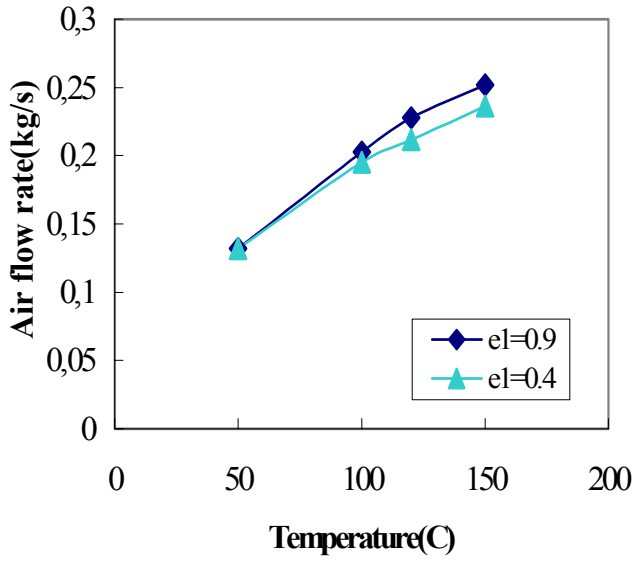

Figure 3.27 : Air mass flow rate for different emissivity

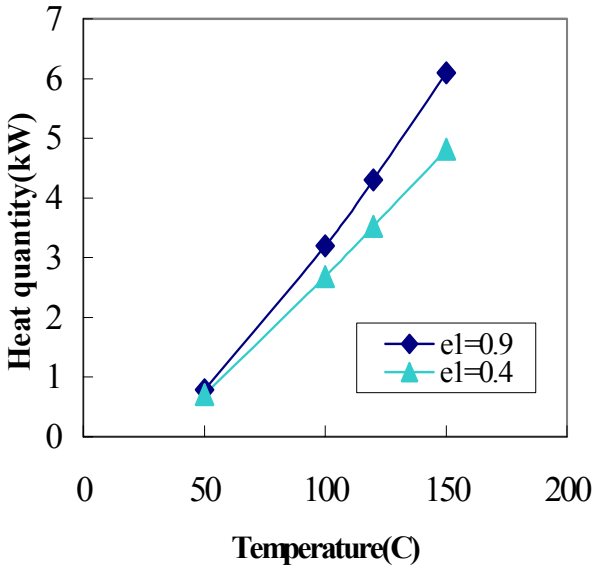

Figure 3.28 : Removed heat for different emissivity

3.4 Effect of the baffle

Figure 3.29 and figure 3.30 compare the air temperature and the air velocity at the outlet mid-line(Y=0.25m)for three different tests,i.e.with a thermally insulating baffle or a thermally

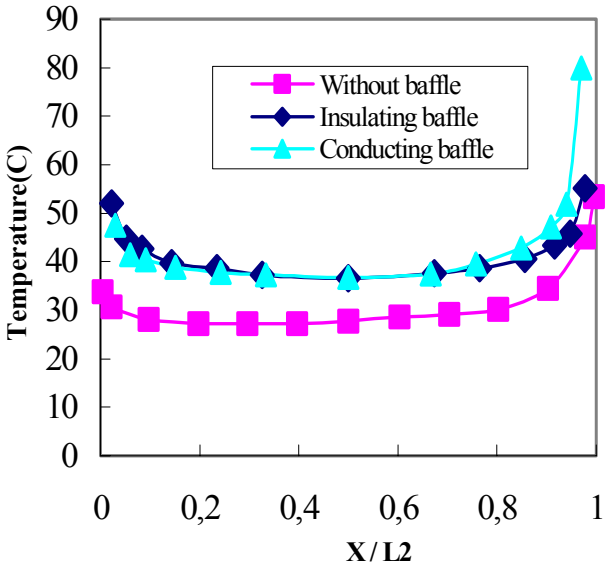

Figure 3.29 : Air temperature distribution (Y=250 mm)

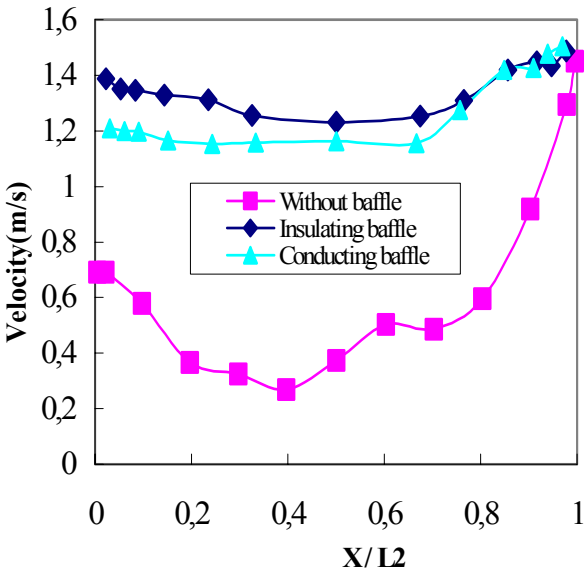

Figure 3.30 : Air velocity distribution (Y=250 mm)

conducting baffle, without baffle [3], respectively. The test parameters are as below: heated height 8.0 m, hot channel dimension 330×500 (mm), heated wall temperature 150 ^{0}C, the emissivity of the side wall 0.4, the emissivities of other walls 0.9, inlet air temperature 20^{0}C. It is seen that the outlet air temperature and air velocity for the test with a baffle is much higher than that without a baffle. The thermal conductivity of the baffle affects only slightly the temperature and the velocity profile. In case with a thermally insulating baffle, the air velocity is higher than that in case with a thermally conducting baffle.

Figure 3.31 represents the baffle temperature at Z=3m and the back wall temperature at Z=3.8m for the same test parameters as indicated in figure 3.29. It is found that the temperature of the thermally insulating baffle is clearly higher than that of the thermally conducting baffle. The back wall temperature without baffle is much higher than that with a baffle. The back wall temperature with a thermally conducting baffle is slightly higher compared to that with a thermally insulating baffle.

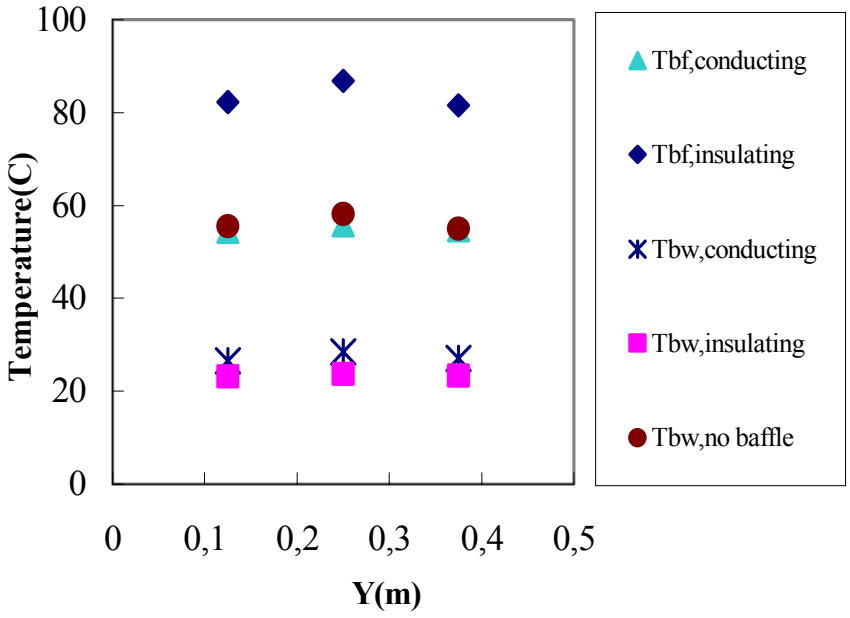

Figure 3.31 : Baffle temperature and back wall temperature

Figure 3.32 shows the air flow rates for three different tests, the test conditions are the same as indicated in figure 3.29. It is seen that the outlet air mass flow rate is much lower by using any baffle, but the thermal conductivity of the baffle affects only slightly the air flow rate. Figure 3.33 compares the total removed heat for the same test parameters as in figure 3.32. It's found that the effect of the baffle type on the removed heat power is negligibly small.

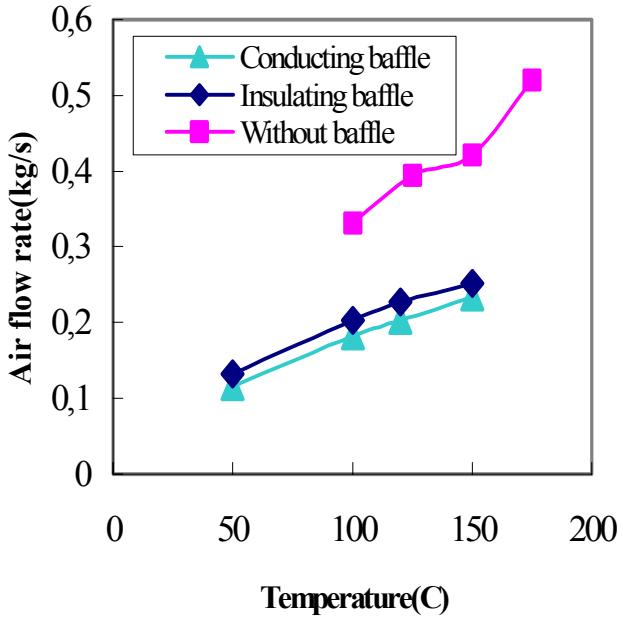

Figure 3.32 : Air mass flow rate for different baffle

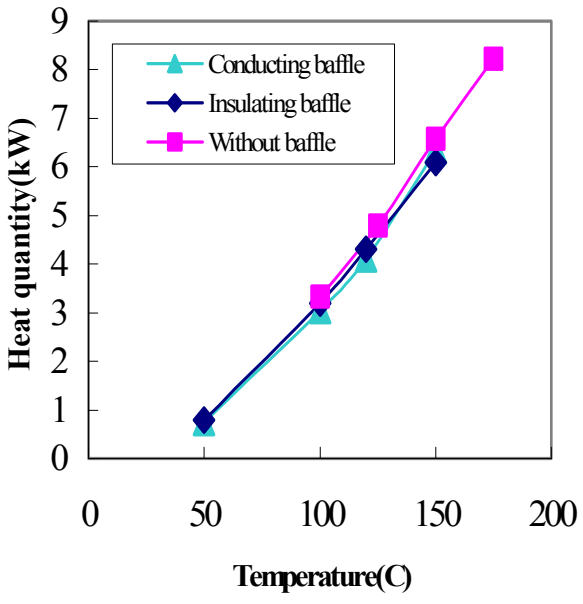

Figure 3.33 : Removed heat for different baffle

3.5 Test results under the wet conditions

Figure 3.34 and figure 3.35 show the mean temperature on the heated wall and on the baffle

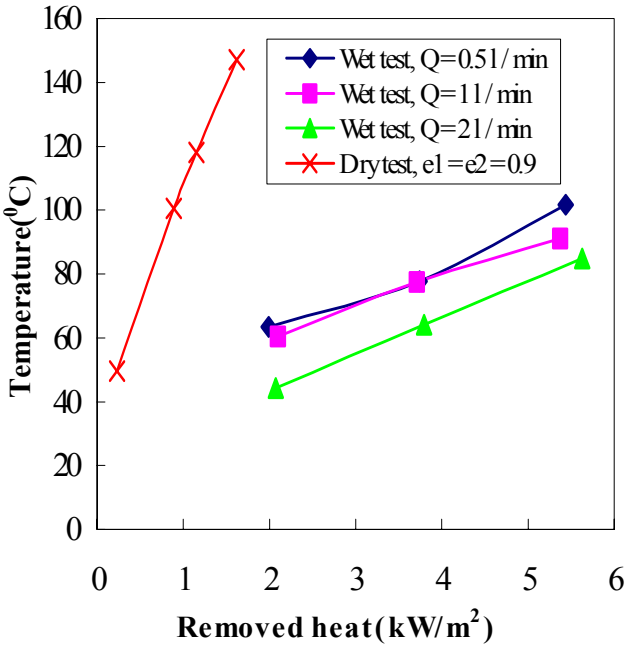

Figure 3.34 : Mean temperature on the heated wall

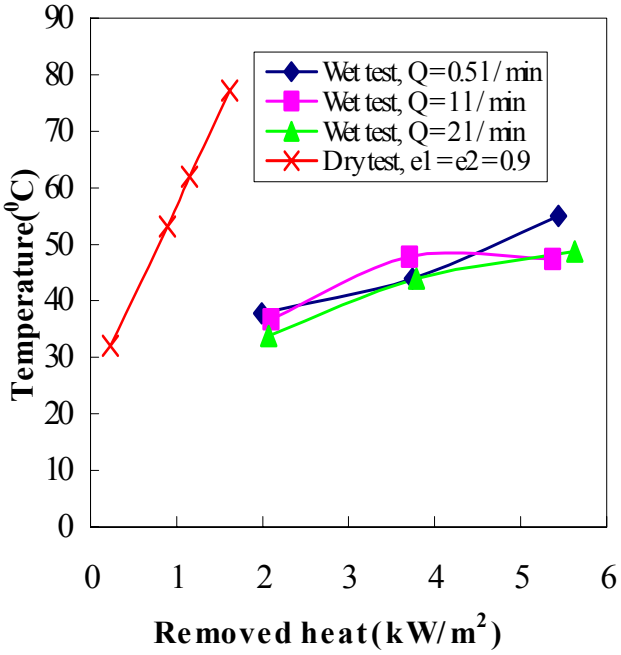

Figure 3.35 : Mean temperature on the baffle

versus the removed heat power for three wet test conditions, i.e. the water flow rate 0.5 l/min, 1.0 l/min and 2.0 l/min. The results under the dry conditions with an insulating baffle are also presented in these two figures. The hot channel dimension is 420×500 (mm). It is seen that the mean temperature on the heated wall and on the baffle for the tests under the wet conditions are much lower than that under the dry conditions at the same power level. The mean temperature on the heated wall and on the baffle increase by increasing the removed heat power at the same water flow rate. Generally, the mean temperature on the heated wall decreases by increasing the water flow rate.

3.6 Water film observation

Figure 3.36 and figure 3.37 shows the water film on the heated wall with two different coating materials without heat input. The water flow rate is about 1.5~2.0 l/min. The coating materials are Carbo Zinc® and EISENGLIMMER(e1=0.9), respectively. Obviously, Carbo Zinc® improves the formation of the water film significantly.

Figure 3.36: Water film on the heated wall with Carbo Zinc®

Figure 3.37: Water film on the heated wall with EISENGLIMMER

4. Numerical simulation

4.1 FLUTAN code

Numerical simulation of 3-D turbulent natural convection coupled with thermal radiation required high capabilities of a computer code. In the present study the FLUTAN3.0 code [4] is used which is developed at the Research Center Karlsruhe. FLUTAN is a highly capable computer code for 3-D fluid dynamic and thermal-hydraulic analyses in Cartesian or cylinder coordinates. It's related to the family of the COMMIX code originally developed at Argonne National Laboratory. FLUTAN 3.0 code is an improved version of the FLUTAN code released in 1998. In comparison to the old version it offers some additional innovations, e.g. the QUICK-FRAM techniques for reducing numerical diffusion in the k- ε turbulence model. The pressure condition has been revised and upgraded to fully include the outlet volume cells in the computational process, i.e. to promote the solution of the conservation equations for all nodes within the defined model boundary surface. A so-called visualization option based on VISART standards has been provided as a post-processing tool. A turbulent model for buoyant flows, local grid refinement, and a 3-D heat conduction model for structures have been added to the code.

A thermal radiation model has been developed to determine the radiative heat exchange between solid walls. The radiation equations are solved either directly or iteratively. In order to reduce the storage need and computing time and to improve the numerical efficiency, the so-called macro-element method has been developed and implemented into the FLUTAN code [5].

According to the experiments at the PASCO test facility, it is needed to modify the thermal radiation model and to add new thermal radiation boundary conditions to the FLUTAN code. In the present PASCO experiments, no radiative heat exchange takes place between the walls in the cold channel and that in hot channel due to the baffle. In this case, a criterion is set up in the FLUTAN code to determine whether there is radiative heat exchange between two surface elements. Heat conduction through the baffle has to be taken into account. The radiation boundary conditions on the baffle surfaces are changed, because the heat transferred by air convection is not equal to the heat transferred by thermal radiation.

4.2 Results with an insulating baffle

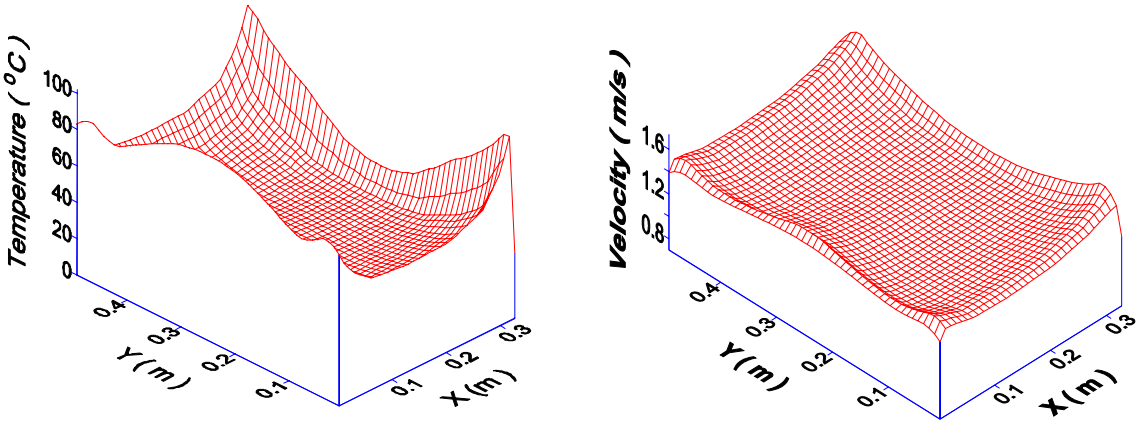

(a) Air temperature (b) Air velocity

Figure 4.1: Profile of the air temperature and the air velocity at the outlet cross-section

Figure 4.1 shows the profile of the air temperature and the air velocity at the outlet cross-section in the hot channel for the reference conditions with an insulating baffle. It can be seen that the air temperature decreases rapidly with the distance from the heated wall. The maximum temperature locates in the corner where the heated wall connects with the side wall. Because of thermal radiation between the walls, the air temperature increases again by approaching the baffle. The minimum temperature locates in the central region. In comparison with the air temperature profile, the air velocity distribution has the similar results. The minimum value of the air velocity appears in the central region.

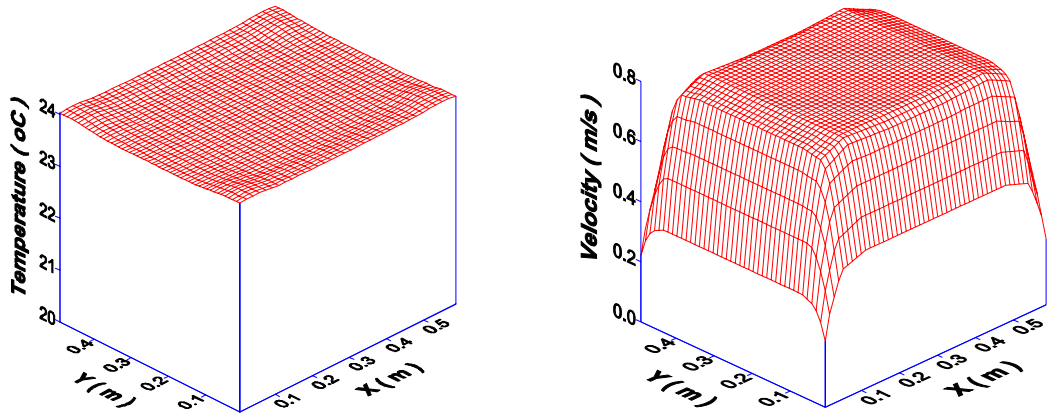

(a) Air temperature (b) Air velocity

Figure 4.2: Profile of the air temperature and the air velocity at the inlet cross-section

Figure 4.2 shows the profiles of the air temperature and air velocity at the inlet cross-section for the reference conditions with an insulating baffle. The air temperature distribution is

Figure 4.4 indicates the distributions of the convective heat flux and the radiative heat flux on the heated wall for the reference condition with an insulating baffle. Due to the lower air temperature and the undeveloped boundary layer the convective heat flux in the inlet region of the hot channel is much higher than the other regions, where the convective heat flux remains nearly uniform. It increases again near the outlet region. The radiative heat flux decreases gradually with the increasing axial level except for that in the outlet region, where more heat is radiated to the environment.

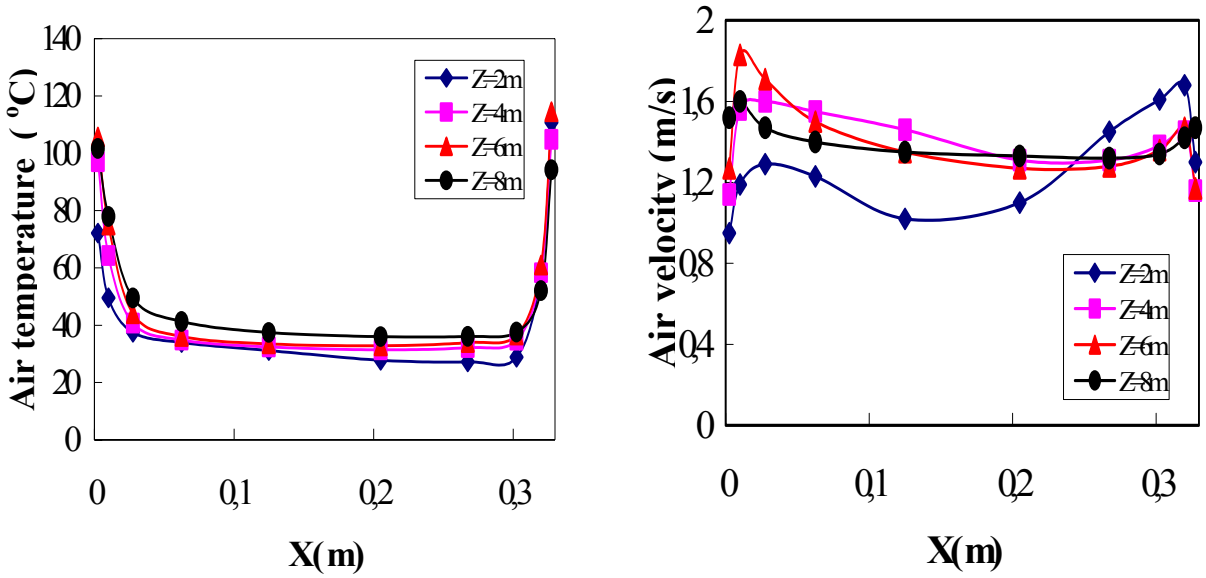

(a) Air temperature (b) Air velocity

Figure 4.5: The air temperature and the velocity distribution along the mid-line (Y=0.25 m) in the hot channel

Figure 4.5 presents the air temperature and the air velocity along the middle line (Y=0.25 m) versus the distance from the baffle at different axial levels in the hot channel for the reference condition with an insulating baffle. Higher the axial level is, higher the air temperature is. The air temperature increases rapidly near the heated wall and the baffle. At the middle region the air temperature distributes nearly uniformly. At Z=2 m the velocity near the baffle is much lower due to strong eddy effect in the inlet region. At high axial level the air velocity is more uniform and increases near the walls.

4.3 Results with a conducting baffle

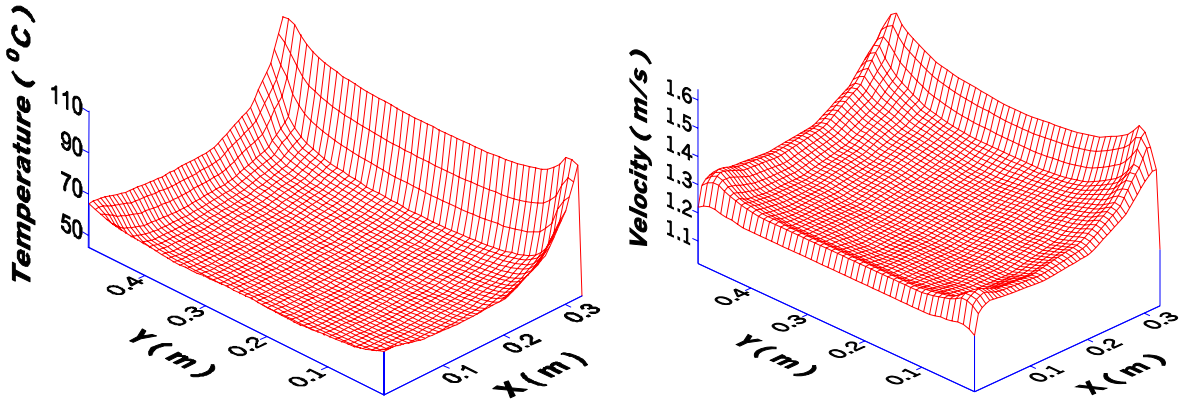

(a) Air temperature (b) Air velocity

Figure 4.6: Distribution of the air temperature and the air velocity at the outlet cross-section in the hot channel

Figure 4.6 shows the distributions of the air temperature and the air velocity at the outlet cross-section in the hot channel for the reference condition with a conducting baffle.

It can be seen that the air temperature decreases rapidly with the distance from the heated wall. The maximum temperature locates in the corner where the heated wall connects with the side wall. In comparison with the insulating baffle the air temperature distribution is more non-uniform. The air temperature is much lower near the baffle than that near the heated wall due to lower baffle temperature. Because of thermal radiation between the walls the air temperature increases again near the side wall. The minimum value of the air temperature appears close to the baffle. The similar results can be obtained for the air velocity distribution.

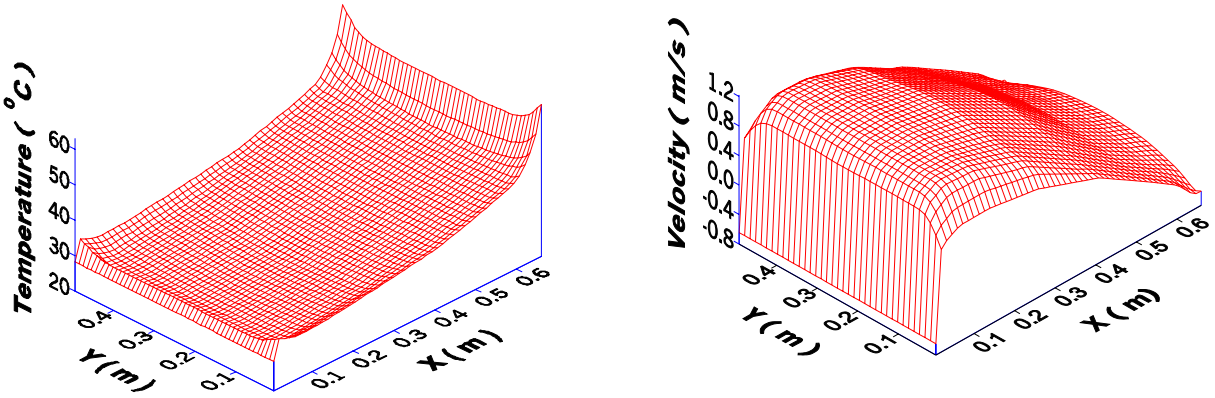

(a) Air temperature (b) Air velocity

Figure 4.7: Distribution of the air temperature and the air velocity at the inlet cross-section

temperature increases again near the side wall. The minimum value of the air temperature appears close to the baffle. The similar results can be obtained for the air velocity distribution.

Figures 4.7 shows the profile of the air temperature and the air velocity at the inlet cross-section for the reference condition with a conducting baffle.

The air temperature increases with the distance from the back wall to the baffle. In comparison with the results with an insulating baffle the air temperature near the baffle is much higher due to the heat conduction from the hot side to the cold side of the baffle. The air velocity near the baffle is negative. It means that air changes its flow direction and flows upward in that region. This is due to the strong buoyancy effect in this region, which leads to a local flow re-circulation. The maximum value of the upward velocity is about 0.65 m/s.

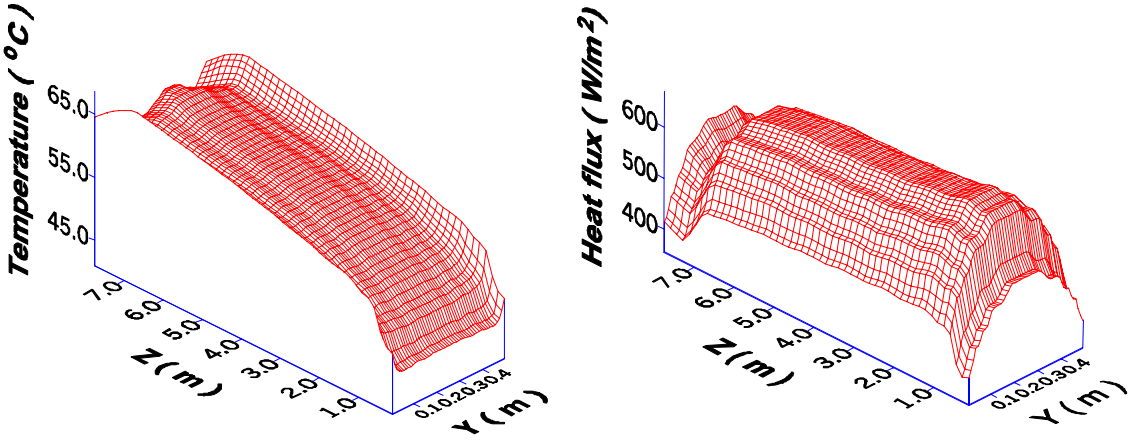

(a) Baffle temperature (b) Radiative heat flux

Figure 4.8: Profile of the temperature and the radiative heat flux on the baffle

Figure 4.8(a) shows the temperature distribution on the baffle in the hot channel for the reference condition with a conducting baffle. At the same axial level the temperature is nearly uniform. The temperature increases with increasing axial level because the increase in the air temperature. But at the outlet region the temperature decreases again due to heat loss into the ambient air. By comparing with the test with an insulating baffle, the temperature is much lower because the baffle is also cooled by cold channel air. Figure 4.8(b) indicates the profile of the radiative heat flux on the baffle. The radiative heat flux is hardly changed with the axial elevation except for the outlet and the inlet regions, where the radiative heat flux is lower due to the radiative heat loss. At the same axial level the radiative heat flux is higher in the central region than in the regions near the walls.

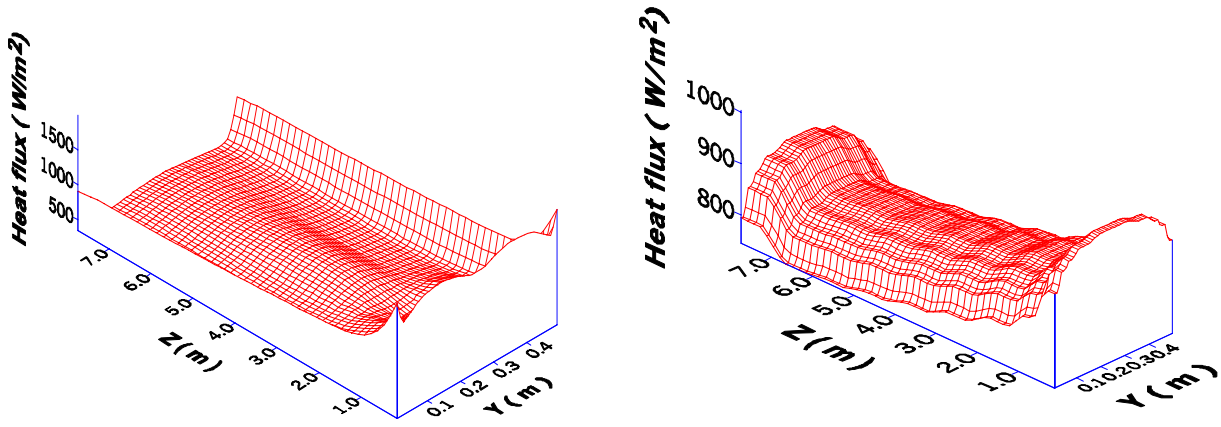

(a) Convective heat flux (b) Radiative heat flux

Figure 4.9: Profile of the convective and the radiative heat flux on the heated wall

Figure 4.9 shows the distribution of the convective heat flux and the radiative heat flux on the heated wall for the reference condition with a conducting baffle. The convective heat flux distribution is similar to that with an insulating baffle. The radiative heat flux distribution is quite different from that with an insulating baffle. The radiative heat flux is much higher in the outlet and in the inlet regions than in the middle region.

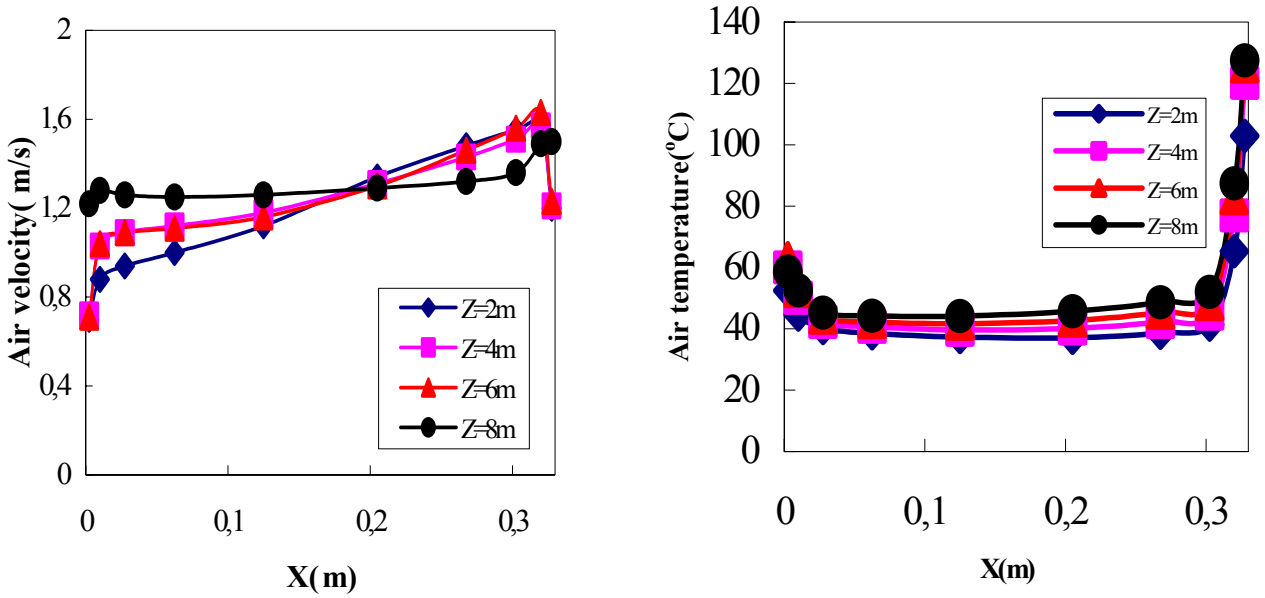

(a) Air velocity (b) Air temperature

Figure 4.10: Air temperature and Air velocity along the mid-line (Y=0.25 m) in the hot channel

Figure 4.10 presents the air velocity and the air temperature along the middle line (Y=0.25 m) versus the distance from the baffle at different axial levels for the reference condition with a conducting baffle. The air temperature increases rapidly near the heated wall. However, the air temperature is much lower in the region close to the baffle. In the middle region the air temperature distribution is nearly uniform. The distribution of the air velocity distribution is more non-uniform at low axial level. At the same axial level the air velocity near the baffle is lower than that near the heated wall. At high axial level the air velocity distributes more uniformly.

4.4 Effect of the heated wall temperature

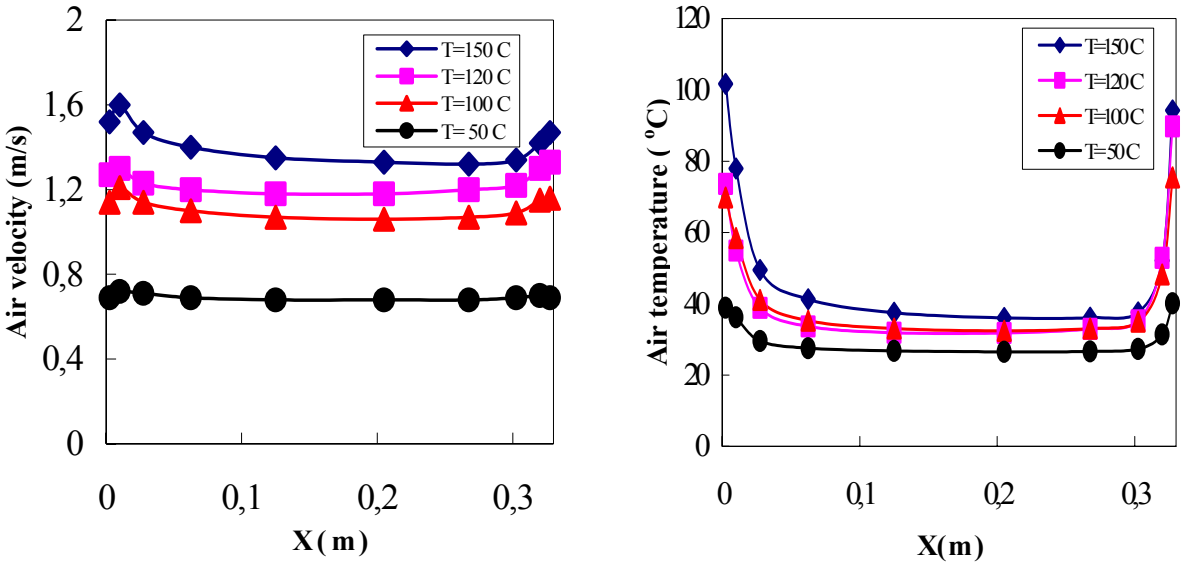

(a) Air velocity (b) Air temperature

Figure 4.11: Air velocity and air temperature along the mid-line (Y=0.25 m) in the hot channel

Figure 4.11 shows the air velocity and the air temperature versus the distance from the baffle for different heated wall temperatures for the reference condition with an insulating baffle. By increasing the temperature of the heated wall the air velocity increases. For the same heated wall temperature the air velocity is higher near the walls than the middle region, where the distribution of the air velocity is well uniform, especially at a low heated wall temperature. The air temperature increases rapidly near the walls. At T=150 C, the air temperature near the baffle is higher than that near the heated wall

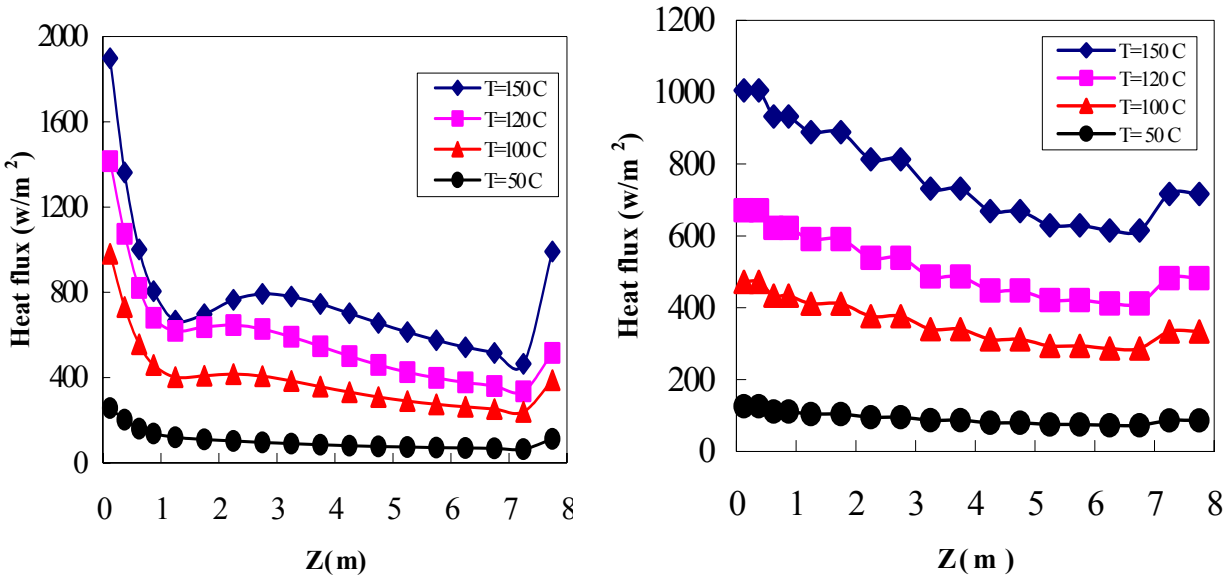

(a) Convective heat flux (b) Radiative heat flux

Figure 4.12: Convective and radiative heat flux on the heated wall along the mid-line (Y=0.25m)

Figure 4.12 shows the convective and the radiative heat flux on the heated wall versus the axial level for the reference condition with an insulating baffle. The convective heat flux is higher in the inlet and the outlet region than that in the middle region. By increasing the heated wall temperature from 50 C to 150 C the convective heat flux increases by about 640%. The radiative heat flux decreases with the distance from the hot channel inlet except for that in the outlet region. Increasing the heated wall temperature from 50 C to 150 C results in a increment about 730% in the radiative heat flux. By increasing the heated wall temperature both of the convection and radiation on the heated wall are enhanced.

4.5 Effect of the hot channel depth

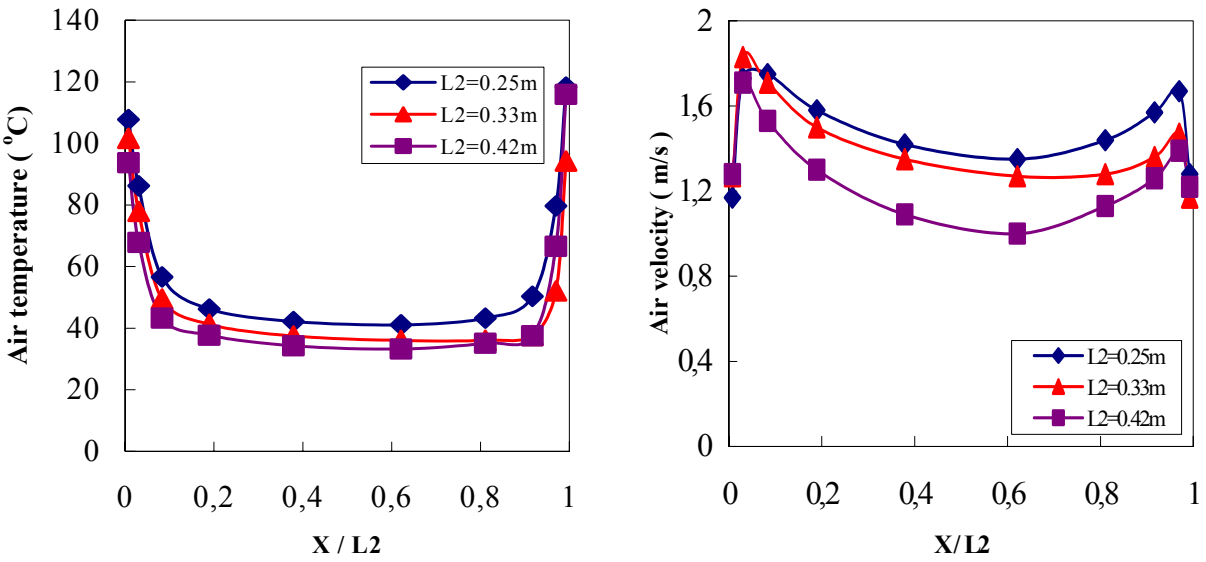

(a) Air temperature (b) Air velocity

Figure 4.13: Air temperature and air velocity distribution along the mid-line (Y=0.25 m) at the outlet cross-section of the hot channel

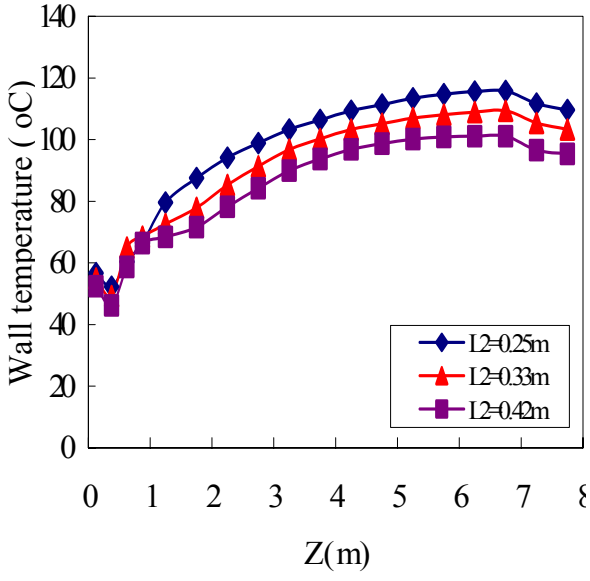

Figure 4.14: Distribution of the temperature on the baffle at Y=0.25 m

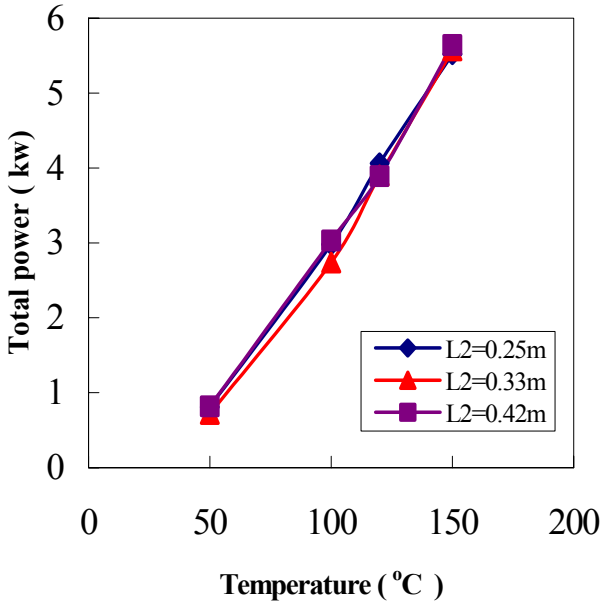

Figure 4.15: Total power versus the heated wall temperature

Figure 4.13 shows the air temperature and the air velocity along the mid-line at the outlet cross-section of the hot channel versus the distance (X/L2) from the baffle in the hot channel for the reference condition with an insulating baffle. The air temperature increases rapidly near the solid walls. At the middle region, the air temperature is nearly uniform. In generally, by increasing the hot channel depth from 0.25m to 0.42m the air temperature has a reduction. By reducing the depth of the hot channel from 0.42m to 0.25m the air velocity increases.

Figure 4.14 shows the baffle temperature versus the axial level for the reference condition with an insulating baffle. The baffle temperature decreases by enlarging the depth of the hot channel due to enhanced thermal radiation. Figure 4.15 shows the total heat power versus the heated wall temperature with different value of the hot channel depth for the reference condition with an insulating baffle. By reducing the channel width from 0.42m to 0.25m, the whole heat power is nearly the same.

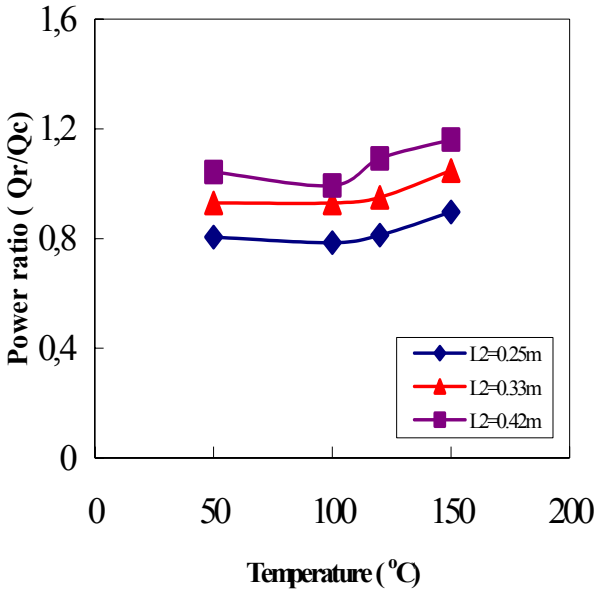

Figure 4.16: Power ratio versus the heated wall temperature

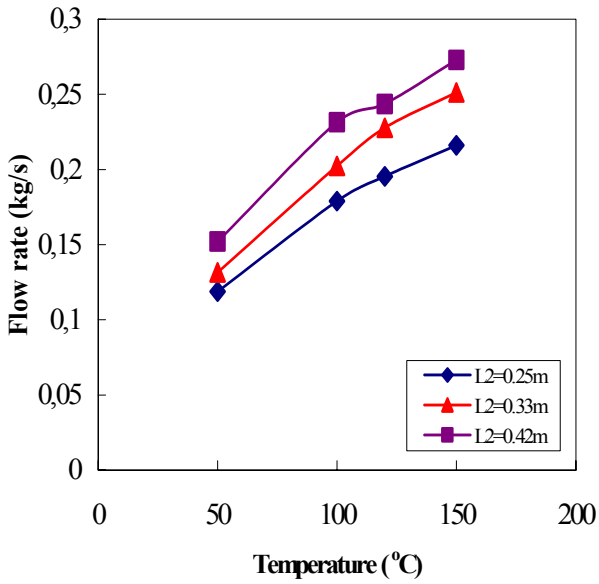

Figure 4.17: Air flow rate versus the heated wall temperature

Figure 4.16 shows the power ratio of the heat power transferred by thermal radiation to the heat power transferred directly by convection versus the heated wall temperature with different hot channel depths for the reference condition with an insulating baffle. For the hot channel depth about 0.25m the ratio is about 0.8. In the case the heat transferred from heated wall by

thermal radiation is less than that by convection. The ratio increases by increasing the hot channel depth. At depth of 0.42 m, the ratio is greater than 1.0. It means the heat transferred by radiation is more than that by convection.

Figure 4.17 shows the flow rate of the air versus the heated wall temperature with the different values of the hot channel depth for the reference condition with an insulating baffle. Decreasing the heated wall temperature from 150 C to 50 C results in a reduction of the flow rate of the air by about 50%. By increasing the hot channel depth from 0.25m to 0.42m the flow rate of the air increases by about 25%. Higher the hot channel depth is, higher the flow rate of the air is.

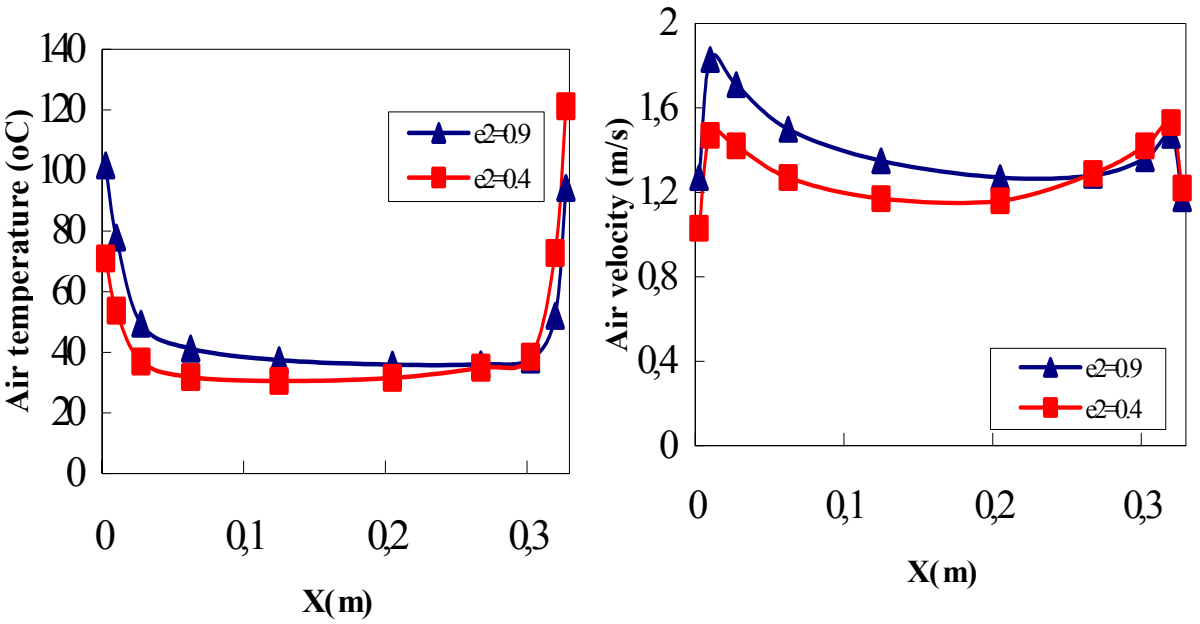

(a) Air temperature (b) Air velocity

Figure 4.18: Profile of the air temperature and the air velocity along the mid-line (Y=0.25m) at the outlet cross-section of the hot channel

Figure 4.18 shows the air temperature and the air velocity at the outlet cross-section versus the distance from the baffle in the hot channel with an insulating baffle. By decreasing the heated wall emissivity from 0.9 to 0.4 the air temperature near the baffle decreases about 30 C due to the less radiative heat transfer to the baffle. Reducing the heated wall emissivity from 0.9 to 0.4 results in the air velocity drops near the baffle. The air velocity is nearly equal near the heated wall with the different emissivity.

4.6 Effect of the heated wall emissivity

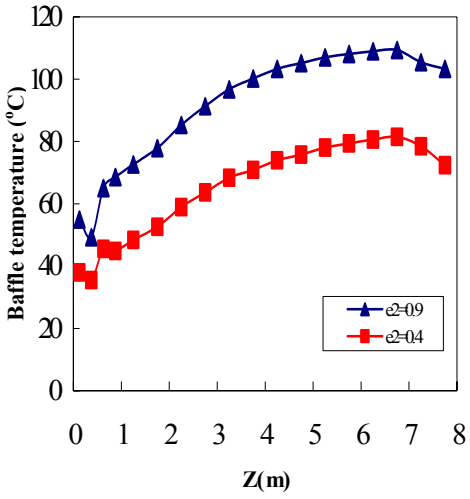

Figure 4.19: Baffle temperature along the mid-line (Y=0.25m)

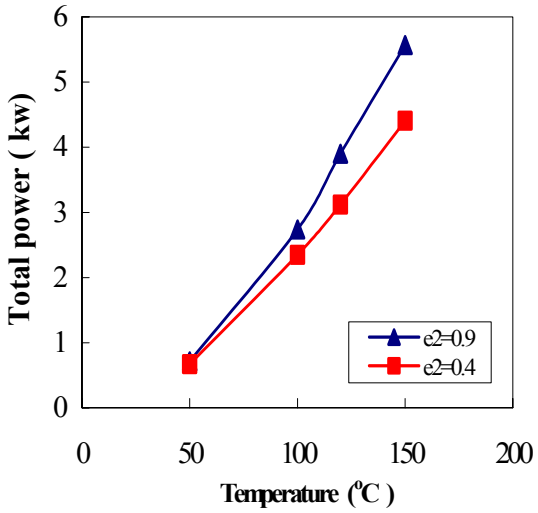

Figure 4.20: Total power versus the heated wall temperature

Figure 4.19 shows the baffle temperature versus the axial level for the reference condition with an insulating baffle. Reducing the heated wall emissivity from 0.9 to 0.4 results in a reduction of baffle temperature about 28 C.

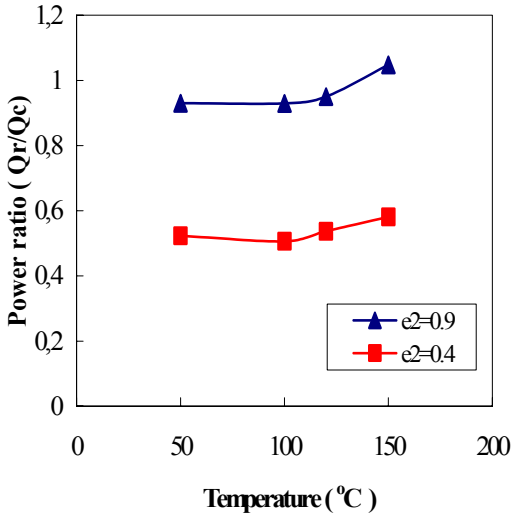

Figure 4.21: Power ratio versus the heated wall temperature

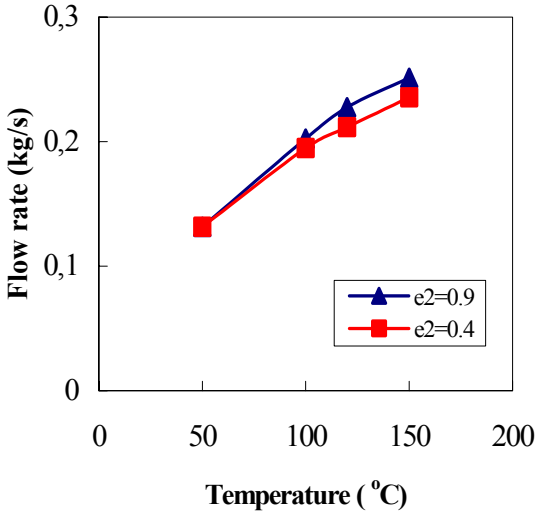

Figure 4.22: Air flow rate versus the heated wall temperature

Figure 4.20 shows the total heat power versus the heated wall temperature with different wall emissivities for the reference condition. By reducing the heated wall emissivity from 0.9 to 0.4 the total heat power decreases by about 20%. By increasing the heated wall temperature from 50 C to 150 C the total heat power increases by about 640%.

Figure 4.21 shows the power ratio of the heat power transferred by thermal radiation to the heat power transferred directly by convection versus the heated wall temperature with different wall emissivities for the reference condition with an insulating baffle. At heated wall emissivity 0.9, the ratio is about 1.0. In this case the heat transferred from heated wall by thermal radiation is equal to that by convection. By reducing the heated wall emissivity from 0.9 to 0.4 the ratio obviously decreases and the value is about 0.5. It means the heat transferred by radiation is half of that by convection. The ratio has nearly same distribution with different baffle emissivities.

Figure 4.22 shows the flow rate of the air versus the heated wall temperature with the different values of the heated wall emissivity for the reference condition with an insulating baffle. The flow rate of the air increases with increasing the heated wall temperature. For the heated wall temperature of 150 C the flow rate of the air with high wall emissivity (0.9) is more than that with low wall emissivity (0.4) by 6%.

4.7 Effect of the baffle type

Figure 4.23 (a) shows the air temperature and the air velocity at the inlet cross-section versus the distance from the back wall (X/L1) in the cold channel for the reference condition. For the case with a conducting baffle, the air temperature is higher than for the case with an insulating baffle, especially at the region near the baffle. Figure 4.23 (b) illustrates the air velocity at inlet cross-section versus the distance from the back wall in the cold channel. The distribution of the air velocity is a typical turbulent profile with an insulating baffle. But with a conducting baffle the flow re-circulation occurs near the baffle. This is due to the buoyancy effect resulted by the high temperature on the baffle.

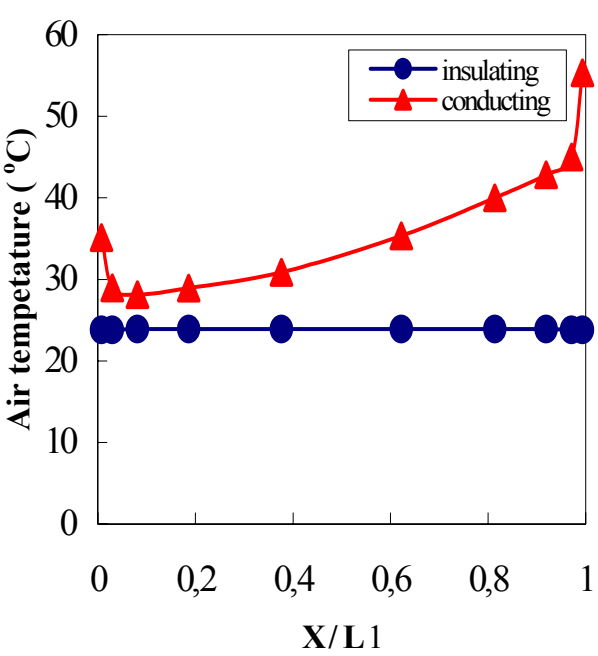

(a) Air temperature

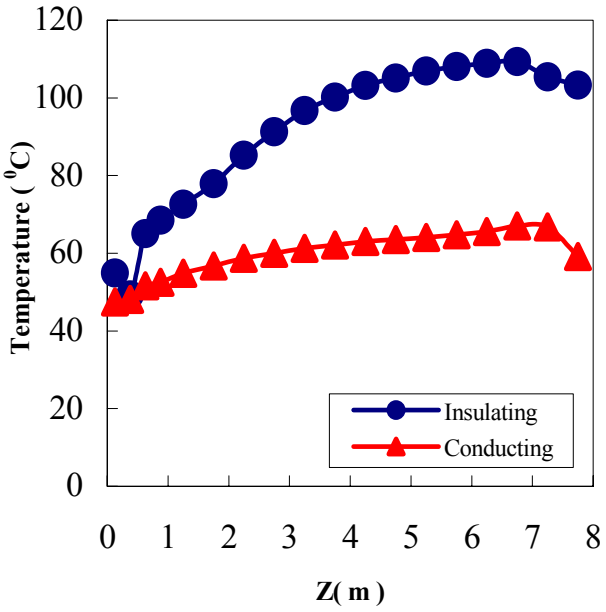

(b) Air velocity

Figure 4.23: Distribution of the air temperature and the air velocity along the mid-line (Y=0.25m) at the inlet cross-section of the cold channel

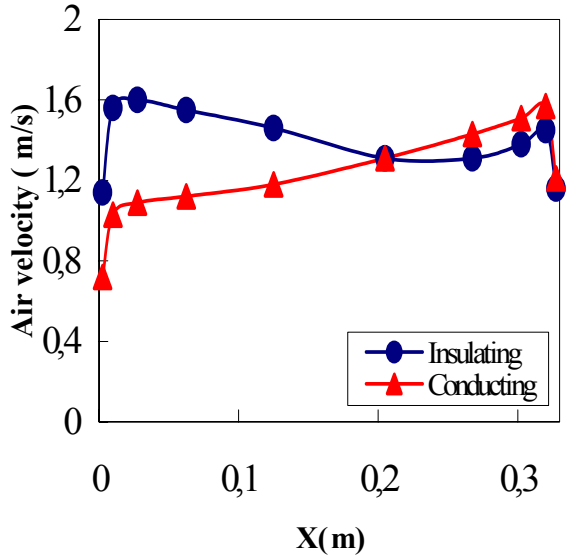

(a) Air velocity

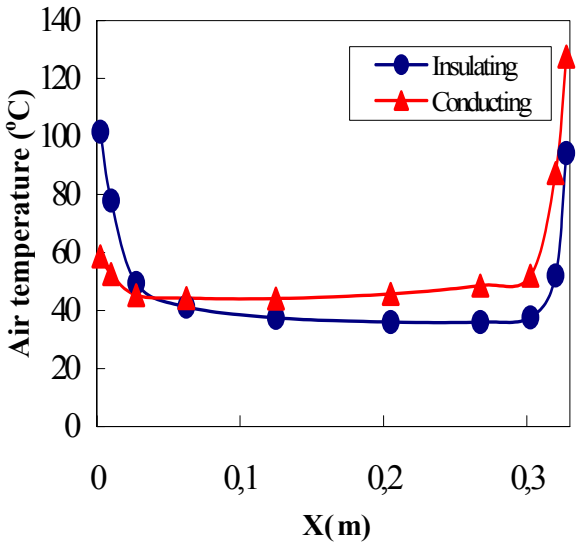

(b) Air temperature

Figure 4.24: Profile of the air velocity and temperature along the mid-line (Y=0.25m) at the outlet cross-section of the hot channel

Figure 4.24 shows the air velocity and the air temperature at outlet cross-section versus the distance from the baffle for the reference condition. The air velocity is much lower with a conducting baffle comparing to that with an insulating baffle in the region close to the baffle. Near the heated wall the effect of the baffle type is small. With a conducting baffle the air temperature in the region near the baffle is much lower than that with an insulating baffle. It is due to the baffle is cooled by the air in the cold channel. Near the heated wall the air temperature is higher with a conducting baffle.

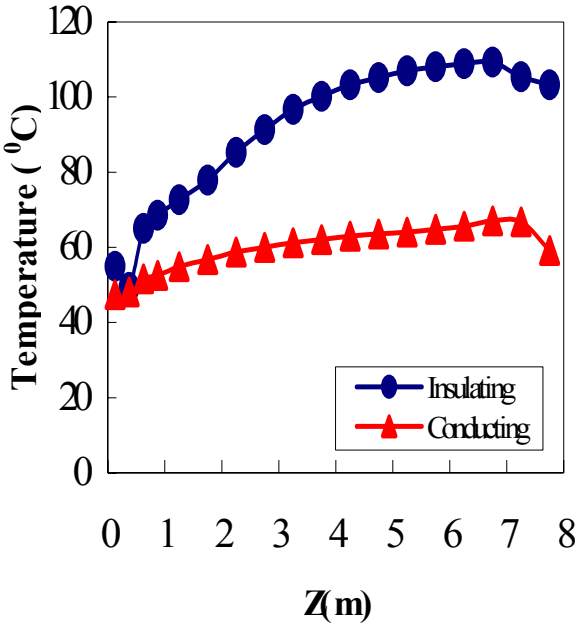

Figure 4.25: Temperature on the baffle along the mid-line (Y=0.25m)

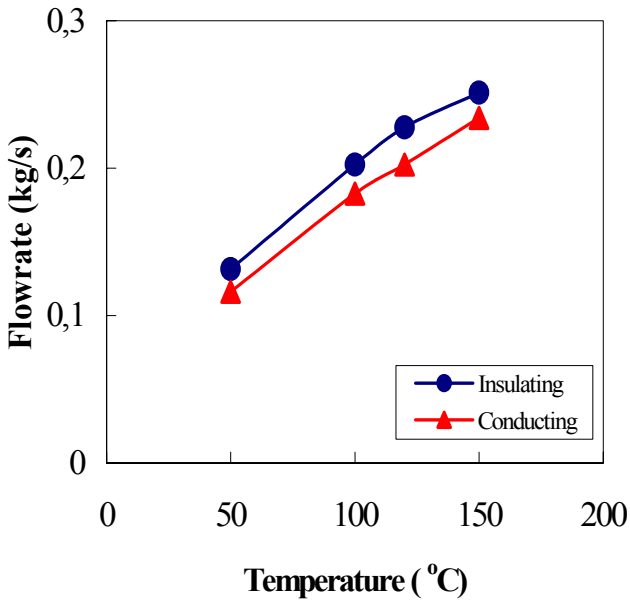

Figure 4.26: Air flow rate versus the heated wall temperature

Figure 4.25 shows the baffle temperature along the mid-line (Y=0.25m) versus the axial level with different baffles for the reference condition. The temperature on a conducting baffle is quite lower comparing with that on an insulating baffle because more heat is transferred into the air in the cold channel in this case.

Figure 4.26 shows the flow rate of the air versus the heated wall temperature with different baffles for the reference condition. The flow rate of the air increases with increasing the heated wall temperature no matter which type the baffle is. The flow rate of the air with a conducting baffle is less than that with an insulating baffle. E.g., for the heated wall temperature of 150 C the flow rate of the air with a conducting baffle decreases by about 8% comparing to that with an insulating baffle.

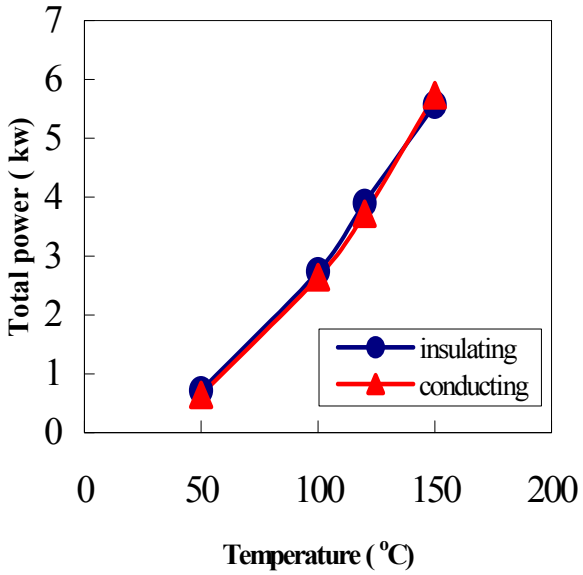

Figure 4.27: Total power versus the heated wall temperature

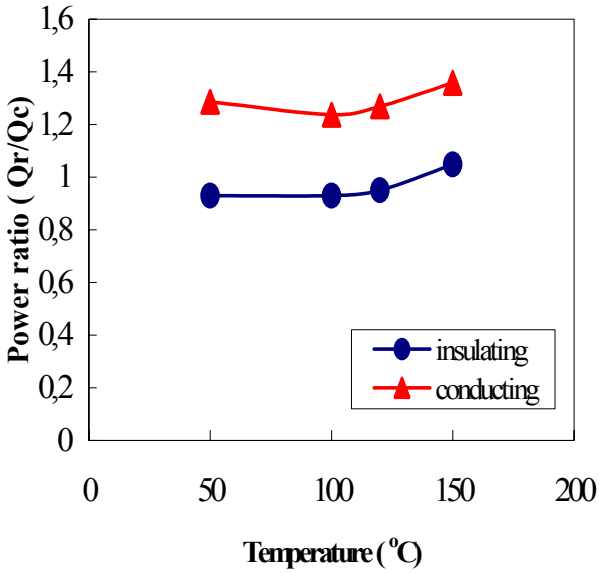

Figure 4.28: Power ratio versus the heated wall temperature

Figure 4.27 shows the total heat power versus the heated wall temperature for two different baffles for the reference condition. In comparison with the insulating baffle the total power almost has no change with conducting baffle.

Figure 4.28 shows the ratio of the heat power transferred by thermal radiation to the heat power transferred directly by convection versus the heated wall temperature for two different baffle types for the reference condition. In comparison with the insulating baffle, the ratio increases for the conductive baffle because more net radiative heat attracted by that baffle. The ratio value is about 1.3. In this case heat transferred from heated wall by thermal radiation is more than that by convection directly.

5 Comparison between the numerical results and the experimental data

Figure 5.1 compares the calculated heat power transferred from the heated wall with the experimental results for different conditions. For all tests points the maximum deviation between the experimental and the numerical results is less than 15%.

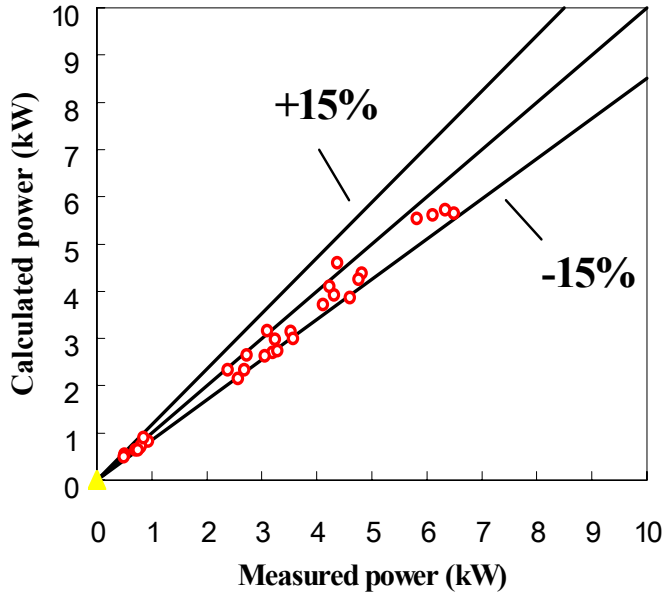

Figure 5.1: Comparison of the calculated power with the measured data

Figure 5.2 and figure 5.3 compare the calculated air temperature and air velocity at the hot

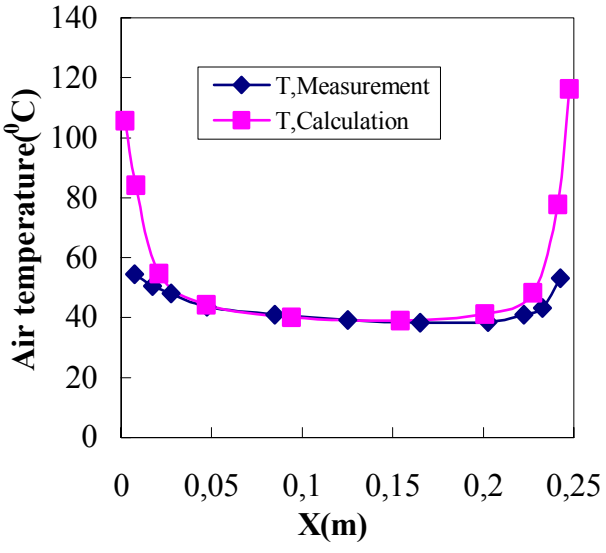

Figure 5.2 : Comparison of the calculated air temperature with the test data

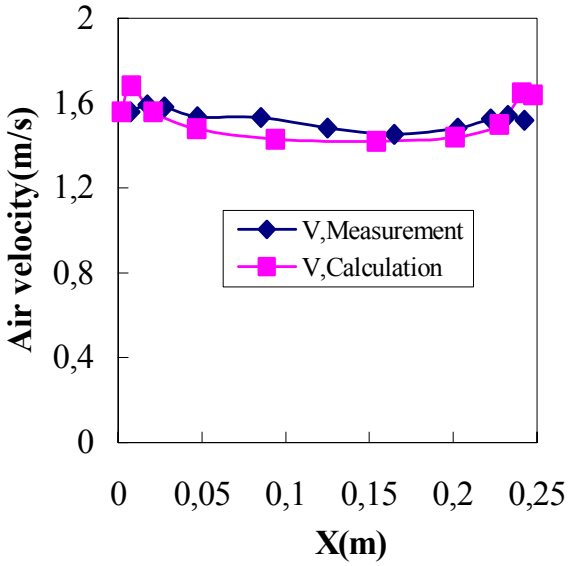

Figure 5.3 : Comparison of the calculated air velocity with the test data

uniform due to the insulating baffle prevents heat transferred from the hot side to the cold side. The air velocity distribution has the typical profile of a turbulent flow. The air velocity in the central region is uniform, whereas it decreases rapidly near the solid walls.

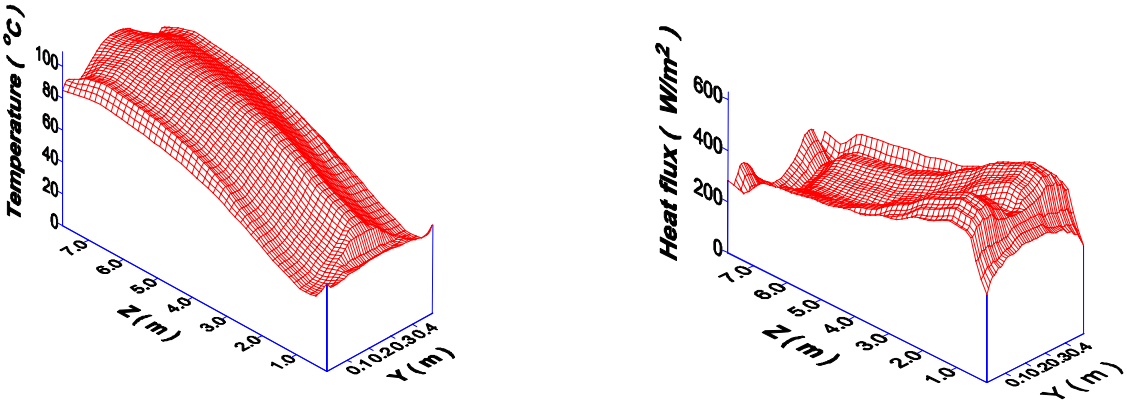

(a) Temperature (b) Radiative heat flux

Figure 4.3: Distribution of the temperature and the radiative heat flux on the baffle

Figure 4.3 shows the temperature and the radiative heat flux distribution on the baffle surface in the hot channel for the reference condition with an insulating baffle. The temperature distribution is symmetric to the line Y=0.25 m. At the same axial level, the temperature is higher at the symmetric axis due to a stronger heat transfer. The temperature increases with increasing the axial level and then decreases again close to the channel outlet because of radiative heat loss to the environment. The radiative heat flux increases rapidly in

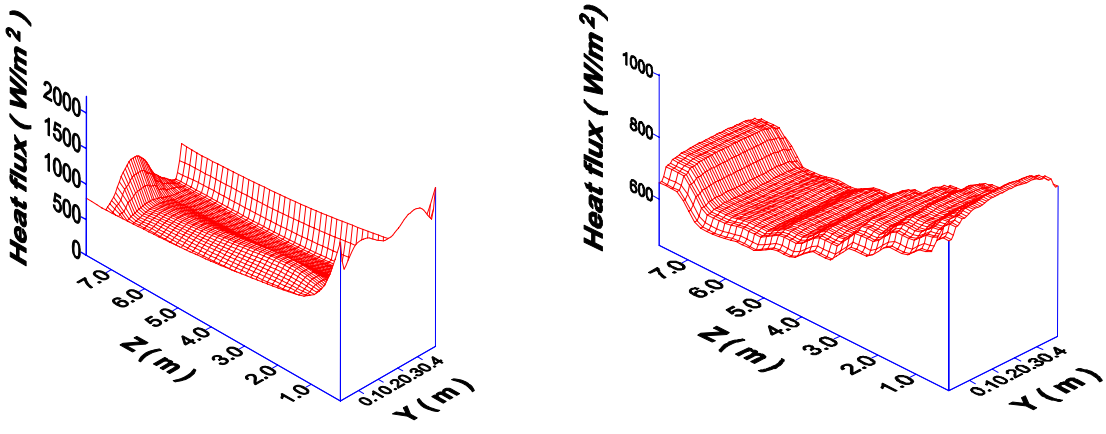

(a) Convective heat flux (b) Radiative heat flux

Figure 4.4: Distribution of the convective and the radiative heat flux on the heated wall

the hot channel inlet due to a lower baffle temperature. The radiative heat flux decreases with the increasing axial level. By approaching the outlet region it increases again.

channel outlet cross-section along the middle line (Y=250mm) with the experimental data. Figure 5.4 shows the measured and the calculated temperature on the baffle along the mid-line (Y=0.25m) versus the axial level. The test parameters are: heated height 8.0 m, hot channel dimension 250×500 (mm), heated wall temperature 150 ^{0}C, the emissivity of the side wall 0.4, the emissivities of other walls 0.9, inlet air temperature 20^{0}C. Generally, A good agreement between the numerical and the experimental results has been found.

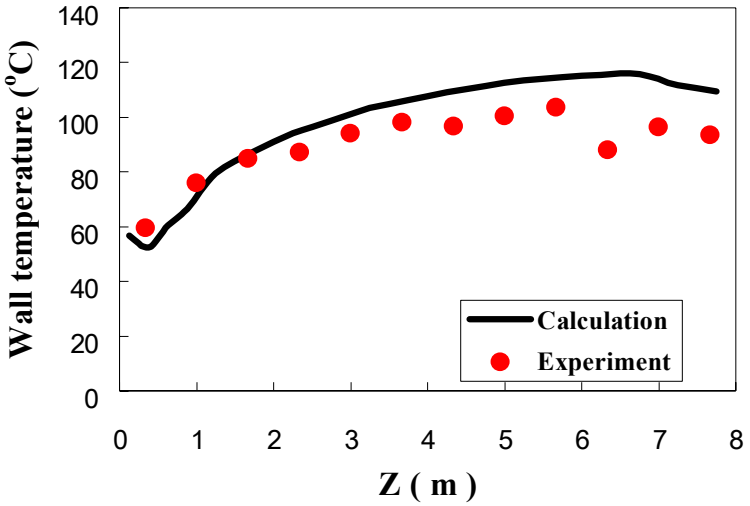

Figure 5.4: Temperature distribution on the baffle

6 Summary

According to the experimental and numerical results obtained so far, the following main conclusions can be drawn:

- A strong influence of thermal radiation occurs on the heat removal under the dry conditions. About 50% of heat is removed from the heated wall by thermal radiation.
- The thermal radiation is strongly affected by the wall emissivity, especially in case that the wall emissivity is high.
- The effect of the channel dimension on the removed heat is negligibly small for the test conditions considered.
- At the test range, the removed heat remains nearly unchanged by using different types of baffles, i.e. a thermally conducting baffle, a thermally insulating baffle or without baffle.
- The removed heat is much higher for test under wet conditions compared to that under the dry conditions at the same mean temperature.
- Generally, there is a uniform distribution of water film on the heated wall with Carbo Zinc® coating material, whereas a strongly non-uniform distribution of water film is observed on the heated wall with the painting material EISENGLIMMER.
- The present results show that the passive containment cooling system with water evaporation, natural air convection and thermal radiation seems to be a feasible concept for AC-PWR.

Acknowledgement

This work was executed under a bilateral co-operation between FZK and NPIC. The authors wish to express their thanks to Professor S.R. Zhang, Professor H. Zhao, Professor B.D. Chen (NPIC), Professor U. Müller and Dr. G. Heusener (FZK) for initiating this co-operation and their support of this work.

Nomenclature

B	:channel width, m
e1	:heated wall emissivity
e2	:baffle emissivity
H	:heated height, m
L1	:cold channel depth, m
L2	:hot channel depth, m
P	:pressure, Pa
Q	:water flow rate, l/min
T	:temperature, °C
V	:velocity, m/s
X, Y, Z	:coordinates, m (mm)
Φ	:humidity, %

Subscripts

0	:inlet
bf	:baffle
bw	:back wall
sw	:side wall

References

[1] V. Berkovich, A. Bianchi, B. Chen, J. Meseth, J. Vecchiarelli, M. Vidard, “Advances in technologies for decay heat removal”, IAEA-SM-353/14

[2] X. Cheng, F. J. Erbacher, H.J. Neitzel, “Passive containment cooling for next generation water cooled reactors”, Proceedings of the ICONE-4 Conference, New Orleans, La., March 10-14, 1996, pp. 343-356

[3] X. Cheng, H.J. Neitzel, H. Schmidt, “Final design report: PASCO Project”, CONT-DABASCO(97)-D006, FZK, December 1997, private communication

[4] G. Groetzbach, L. Carteciano, B. Dorr, “FLUTAN3.0: A computer code for 3-D Fluid and Thermal-Dynamic Analysis in Cartesian and Cylinder Coordinates”, private communcation, FZK, July 2000

[5] X. Cheng, U. Mueller, “Turbulent Natural Convection Coupled with Thermal Radiation in Large Vertical channel With Asymmetric Heating”, Int. J. Heat Mass Transfer, Vol.41 No.12, pp.1681-1692, 1998

[6] Bo Ping, Tan Zuo, “Passive Safety Design for AC600”, Nuclear Power Engineering, Vol. 10(5), P. 19, 1989

[7] Leng Guijun, Yu Hongxing, “AC600 Containment Thermal-hydraulic Analysis”, NPIC report, HDKF1-008Y-BG4, 1998

[8] Li Changlin, “AC600 Core Makeup Tank Test”, NPIC report, AC600A-1-BGA, 1998

[9] Jiang Yuanan, Hu Jun, “AC600 Containment Wind Tunnel Test”, NPIC report, AC600S-1-07, 1994

[10] S. S. Tan, “Test plan of the passive containment cooling system on PASCO test facility”, NPIC report, APR-2-02A, 2000